ZVI-loaded Biochar Composite for Effective Peroxymonosulfate Activation: Application in the Removal of Naphthenic Acids from Real Oil Sands Process Water

by

Adriana Marcela Vasquez Aldana

A thesis submitted in partial fulfillment of the requirements for the degree of

Master of Science

in

Environmental Engineering

Department of Civil and Environmental Engineering
University of Alberta

ABSTRACT

Oil Sands Process Water (OSPW) is a byproduct generated during the extraction of bitumen from oil sands deposits in Northern Alberta, Canada. This matrix presents a critical environmental and industrial challenge due to its toxic nature, primarily associated with its complex mixture of contaminants, notably naphthenic acids (NAs). Consequently, significant efforts have been directed toward developing efficient treatment methods for the remediation and reclamation of OSPW. This thesis investigates for the first time the synergetic effect of coupling peroxymonosulfate (PMS) with a zero-valent iron (ZVI)-loaded biochar (FL600-Fe) derived from pyrolyzed flax straw (FL600-Fe) as a promising method for the efficient degradation of NAs in real OSPW.

Characterization techniques demonstrated the successful incorporation of ZVI particles into the biochar, magnetization properties, and a suitable zeta potential value that helps in the generation of reactive oxygen species due to a positive surface charge. Following adsorption equilibrium experiments and optimal experimental parameters analyses, results indicated that the FL600-Fe/PMS system exhibited a 93.9% degradation efficiency of classical NAs (O_2-NAs) after 120 min using a catalyst and oxidant dose of 1 g L^{-1} and 1 mM, respectively. The radicals responsible for the degradation of NAs were identified as $^{\bullet}OH$, $SO_4^{\bullet-}$ and $O_2^{\bullet-}$ using quenching experiments and electron paramagnetic resonance spectroscopy. The toxicity was evaluated through a 21-hour microbial viability assay, demonstrating a remarkable increase of over 80% in bacterial growth post-treatment. The concentration of bioavailable acid extractable organics that contribute to toxicity in OSPW was reduced by over 70% post-treatment. Furthermore, leaching tests confirmed the stability of the composite biochar, as hardly any iron leaching was detected.

These results suggest that the FL600-Fe/PMS system has high environmental compatibility due to no secondary contamination associated with iron leaching during treatment and toxicity reduction, demonstrating its potential for the treatment of a matrix with a complex chemical composition like OSPW. Additionally, the feedstock used for the composite is a sustainable and renewable material produced from agricultural waste, which makes it a sustainable, cost-effective, and environmentally friendly process for OSPW reclamation.

PREFACE

This thesis presents an original work conducted and documented by Adriana Marcela Vasquez Aldana under the supervision of Dr. Mohamed Gamal El-Din in the Department of Civil and Environmental Engineering at the University of Alberta. The thesis is structured in a paper format, and Chapter 4 serves as a representation of a paper that has been or will be submitted for publication. I conducted the experiments, analyzed the data, and prepared the manuscripts with the guidance of research assistants and post-doctoral fellows in our research group.

DEDICATION

To my parents and little sister, for your encouragement and love. Thank you for being there for me throughout my crazy adventures and dreams.

To all the people who made these two years a wonderful experience and gave their precious time to this project.

ACKNOWLEDGMENTS

Firstly, I would like to express my gratitude to Dr. Mohamed Gamal El-Din for giving me the opportunity to work in his team under his guidance and supervision. His contribution to environmental innovation, extensive knowledge in the field, and commitment to academic excellence have inspired me and challenged me to push beyond my limits. It is an honor to be part of his research group, and I will cherish his mentorship and the impact he has made in my academic career forever.

I would like to acknowledge and give my warmest thanks to Dr. Pamela Chelme-Ayala for her endless support, time, and kindness. Her encouragement, guidance, and advice carried me through all the stages of this journey. I will always appreciate the time she dedicated to discussing my findings and answering my questions. I am immensely grateful to Dr. Isaac Sanchez Montes for playing a key role in this project, thanks to his guidance, knowledge, and proficiency in chemistry and water treatment. I would also like to thank Dr. Lingling Yang for her assistance in data collection, analysis, and interpretation of my data. In addition, my appreciation goes to graduate students and postdoctoral fellows for the hours you have spent providing insightful feedback, engaging in stimulating discussions and offering valuable suggestions to refine my research.

I would like to acknowledge the financial support provided by ICETEX, COLFUTURO Colombia, the University of Alberta's Future Energy Systems research initiative, supported by the Canada First Research Excellence Fund, and the Natural Sciences and Engineering Research Council of Canada (NSERC) Senior Industrial Research Chair (IRC) in Oil Sands Tailings Water Treatment. Finally, I would like to extend my heartfelt gratitude and appreciation to my beloved family for their support, love, and encouragement throughout the journey of completing this thesis.

TABLE OF CONTENTS

LIST OF TABLES

LIST OF FIGURES

CHAPTER 1 Introduction and Research Objectives

1.1 Background and Motivation

1.1.1 Oil Sands Process Water

The oil production and transportation sectors play a significant role in the economy of Canada (Doluweera et al., 2017). This country possesses one of the most substantial oil reserves in the world, ranking fourth globally after Venezuela, Saudi Arabia, and Iran (Government of Alberta, 2023; Oil and Gas Journal, 2022). Notably, the oil production in Alberta accounts for a substantial 80.2% of the total national output (Statistics Canada, 2023). Canada has traditionally employed conventional drilling techniques for crude oil extraction; however, the vast majority of its oil reserves, precisely 97.0%, are situated in the oil sands, mainly in Northern Alberta (Natural Resources Canada, 2022). Moreover, the country holds an impressive 161 billion barrels of remaining established reserves of oil sands that can be recoverable under current technological and economic conditions, and it is estimated that 315 billion barrels more would be recoverable with improved technology (Canadian Association of Petroleum Producers, 2020; Natural Resources Canada, 2023).

It is estimated that the mining method requires around 2.2 barrels of fresh water per barrel of bitumen, with around 78.0% of the water being recycled (Environment and Climate Change Canada, 2021). Nevertheless, reusing water may lead to a reduction in the quality of process water, giving rise to challenges in bitumen recovery as well as the potential for scaling and corrosion in the extraction plant infrastructure (Allen, 2008). Furthermore, due to regulatory frameworks (i.e., zero discharge approach) and the persistency of the complex matrix, oil sands companies are prohibited from discharging oil sands process water (OSPW) into the surrounding environment (Xue et al., 2018). Consequently, one of the biggest challenges in the industry is the accumulation

of billions of m^3 of OSPW in tailings ponds, awaiting effective treatments for water reclamation (Environment and Climate Change Canada, 2021). The volume of OSPW contained in tailings ponds is on the rise, resulting in an estimated accumulation of over 1 billion m^3 spanning across an area exceeding 170 km^2 (Abdalrhman & Gamal El-Din, 2020).

This matrix poses a critical environmental and industrial challenge due to its toxic nature, environmental persistence, and risk of bioaccumulation (C. Li et al., 2017). The potential threat to human health and aquatic life is directly associated with the complex mixture of contaminants present in OSPW, which includes naphthenic acids (NAs), suspended solids, inorganic salts, heavy metals, residual bitumen, and polycyclic aromatic hydrocarbons (Allen, 2008; Lévesque, 2014; Pourrezaei et al., 2014).

1.1.2 Naphthenic Acids

Among the compounds found in OSPW, NAs correspond to a considerable fraction of all organic contaminants and are a primary concern due to their well-documented lethality towards aquatic organisms over other chemical components (Brown & Ulrich, 2015; He et al., 2012; Hughes et al., 2017; Schramm et al., 2000; Wiseman, Anderson, et al., 2013; Wiseman, He, et al., 2013). NAs are compounds naturally occurring in petroleum deposits, resulting from the incomplete degradation of petroleum hydrocarbons by native microbial communities within the reservoirs (Brown & Ulrich, 2015).

These amphiphilic molecules consist of alkyl-substituted cyclo-aliphatic saturated carboxylic acids with acyclic aliphatic acids (paraffinic or fatty), and they become solubilized OSPW during the extraction of bitumen from oil sands (Quinlan & Tam, 2015). NAs are commonly referred to in terms of their structural formula, often expressed as $C_nH_{2n+z}O_x$. In this formula, n represents the carbon number and typically falls within the range of 7 to 26, z indicates

the number of hydrogen deficiencies and can either be zero or a negative number, ranging from 0 to -24, and x denotes the number of oxygen atoms, which can be 2 for classical NAs, and 3 to 6 for oxidized NAs (Abdalrhman & Gamal El-Din, 2020; N. Wang et al., 2013). Additionally, the double bond equivalency (DBE) number (where DBE = 1 – Z/2) is often used to represent the general NAs profiles found in OSPW (Cancelli & Gobas, 2022; R. Huang et al., 2015; Meshref et al., 2017).

The complex composition of OSPW makes the quantification and identification of NAs a challenging analytical task. Many analytical techniques have been studied for the quantification of NAs in OSPW, including Fourier transform ion cyclotron resonance (FT-ICR MS), ion mobility spectrometry (IMS), and ultraperformance liquid chromatography time-of-flight mass spectrometry (UPLC-TOFMS). Although it has a lower resolution, UPLC-TOFMS has demonstrated a similar level of accuracy and precision when compared to high-resolution FT-ICR MS (N. Sun et al., 2014). This approach involves characterizing NAs in a sample by creating a plot that illustrates the relative response associated with each mass corresponding to a specific combination of n and Z (Martin et al., 2008).

1.1.3 OSPW Treatments

The presence of toxic compounds in OSPW, particularly NAs, makes effective treatment a priority. Several treatment processes have been proposed for the degradation of NAs in OSPW, including adsorption (Benally et al., 2019; Islam et al., 2018; Medeiros et al., 2023; Zubot et al., 2012), electro-oxidation (Abdalrhman & Gamal El-Din, 2020), photocatalysis (J. Liu et al., 2016; L. Meng et al., 2023; Suara et al., 2022), and supported biofilters (Arslan et al., 2022; Arslan & Gamal El-Din, 2021).

One of the significant alternatives for OSPW treatment is using advanced oxidation processes (AOPs). AOPs, such as ozonation and ultraviolet (UV) irradiation, have shown promise in degrading NAs and other organic contaminants in OSPW (Demir-Duz et al., 2022; Fang et al., 2018; How et al., 2023; Islam et al., 2014). These methods are based on the generation of highly reactive radicals, such as hydroxyl ($^{\bullet}OH$) and sulfate radicals ($SO_4^{\bullet-}$) by activating oxidants, which can degrade complex organic molecules with high oxidation rates (Quinlan & Tam, 2015). Briefly, oxidants, such as peroxymonosulfate (PMS) or hydrogen peroxide (H_2O_2), can be activated using diverse methods, including UV-C, solar radiation, transition metals or oxides (Deng et al., 2018; S. Li et al., 2022; Sánchez-Montes, O. S. Santos, et al., 2023; Q. Zhao et al., 2017). Various transition metals have been investigated for their efficacy in activating PMS for environmental remediation, with zero-valent iron (ZVI) standing out due to its superior reactivity (Y. Li et al., 2023). However, to address potential challenges such as metal leaching or agglomeration, it is essential to employ a suitable support carrier for this material (S. Wang et al., 2019). Specifically, biochar (BC) has been studied as a substrate for transition metal catalysts (Faheem et al., 2020; Lee & Park, 2020; X. Li et al., 2020; Premarathna et al., 2019). This carbonaceous material is often produced from the pyrolysis of agricultural and forest residues, making it a sustainable, cost-effective, and environmentally friendly method for water treatment (Medeiros et al., 2022). Nevertheless, few studies have applied this promising technology for OSPW remediation (Song et al., 2022). Studying the utilization of BC-Fe composites to activate PMS is crucial for efficient NAs degradation in OSPW.

1.2 Research Scope and Objectives

The significant volume of OSPW generated by the oil sands industry requires treatment to ensure efficient water reclamation and/or safe discharge. Based on previous studies, there have

been no reports about the removal of NAs from real OSPW or model NAs compounds from simulated water using BC-Fe composites as catalysts to activate oxidizing agents. This study reports for the first time the synergistic effect of this system for OSPW remediation. Consequently, the main objective of this research is to develop a BC-Fe composite (named FL600-Fe) derived from flax straw that can efficiently activate PMS for the degradation of NAs in real OSPW.

The specific objectives were to:

(1) Synthesize the ZVI composite catalyst using flax straw as feedstock and $FeCl_3$ as an iron precursor and determine its physicochemical properties by different characterization techniques.

(2) Assess the adsorption equilibrium time between the composite and the fluorophore organic compounds in OSPW.

(3) Determine the effect of catalyst dosage, PMS concentration, and treatment time on the degradation of NAs in real OSPW.

(4) Evaluate the synergetic effect of the FL600-Fe/PMS system compared to control experiments at optimal parameters in degrading NAs from real OSPW.

(5) Identify the main reactive oxygen species generated in the FL600-Fe/PMS system using radical scavengers and electron paramagnetic resonance (EPR) spectroscopy.

(6) Study the potential leaching of iron from the produced ZVI composite during OSPW treatment.

(7) Evaluate the environmental compatibility of the treated OSPW by using a microbial viability assay.

1.3 Hypothesis

It was hypothesized that a BC-Fe composite would be effective in activating PMS to generate radical species that can degrade NAs in real OSPW, resulting in high removal efficiency within a relatively short treatment period (< 3 h).

1.4 Thesis Outline

This thesis is structured into six chapters, with a logical organization corresponding to the outlined research stages and objectives.

Chapter 1 discusses the background information of oil sands in Canada, the OSPW components and environmental concerns, the previously conducted treatments for the remediation of OSPW, research significance, hypothesis, and objectives.

Chapter 2 presents the literature review, including a general introduction to AOPs treatments, PMS activation methods, and biochar as a catalyst carrier.

Chapter 3 describes the experimental methods and materials used throughout the thesis, including chemicals, instruments, and analysis parameters used for composite characterization and OSPW analysis. The experimental setup used for the degradation experiments.

Chapter 4 evaluates the findings found in the material characterization, as well as the results obtained from the experiments of adsorption equilibrium, optimal concentrations for the FL600-Fe/PMS, controls, radical identification, leaching of iron, microbial viability and bioavailability of acid extractable organics that contribute to toxicity before and after treatment.

Chapter 5 provides a general conclusion and summary of the research findings presented in Chapter 4.

Chapter 6 highlights future commendations for further research in this area.

CHAPTER 2 Literature Review

2.1 Advanced Oxidation Processes (AOPs)

Advanced Oxidation Processes (AOPs) are physicochemical treatment techniques used in environmental engineering to effectively degrade organic and inorganic contaminants from wastewater, drinking water, and polluted air (J. Li et al., 2023). The effectiveness of AOPs in decomposing pollutants was acknowledged in the early 70s, prompting extensive research and development efforts aimed at making some of these processes commercially viable (Parsons, 2015). Specifically, AOPs are valuable due to their ability to degrade recalcitrant organic contaminants that are resistant to conventional treatment methods (Ayoub et al., 2010; Tufail et al., 2020). These treatments are typically initiated through the activation of specific oxidizing agents (e.g., ozone, H_2O_2, PMS, peroxydisulfate, and chlorine) by external energy sources (e.g., UV light, solar radiation, and heat) or transition metals, oxides, carbon-based materials, and other materials (Deng et al., 2018; S. Li et al., 2022; Sánchez-Montes, O. S. Santos, et al., 2023; Q. Zhao et al., 2017). One of the main goals of AOPs is to generate highly reactive radical species depending on the oxidizing agent and specific treatment conditions, including $^{\bullet}OH$, $SO_4^{\bullet-}$, superoxide ($O_2^{\bullet-}$), and various reactive chlorine species (e.g., $Cl^{\bullet}$, $Cl_2^{\bullet}$, and $ClO^{\bullet}$) (Hussain et al., 2013; Sánchez-Montes, Santos, et al., 2023). The oxidation potential of various oxidants and some radicals commonly used in water treatment applications are provided in Table 2.1 (Parsons, 2015).

In particular, the $^{\bullet}OH$ is the second most powerful oxidant after fluorine and is non-selective, meaning that it is thermodynamically capable of oxidizing most oxidizable molecules, typically with very high second-rate constants (Buxton et al., 1988; Manasfi, 2021). Furthermore, $^{\bullet}OH$ are short-lived radicals and primarily oxidize organic compounds through processes involving either hydroxylation or hydrogen abstraction. In the course of these reactions, organic radicals are

formed and continually engage with •OH species, ultimately leading to the establishment of the final by-products (Fang et al., 2019; Tang, 2003).

Table 2.1: Oxidation potential of common oxidants (and some radicals) used in water treatment.

Oxidants/radicals	Oxidation Potential (V)
Fluorine	3.03
Hydroxyl radical	2.80
Sulfate radical	2.6
Atomic oxygen	2.42
Persulfate anion	2.12
Ozone	2.07
Peroxymonosulfate	1.82
Hydrogen peroxide	1.78
Perhydroxyl radical	1.70
Permanganate	1.68
Hypobromous acid	1.59
Chlorine dioxide	1.57
Hypochlorous acid	1.49
Chlorine	1.36

Note. Adapted from Advanced Oxidation Processes for Water and Wastewater Treatment by S. Parsons, 2005, IWA Publishing.

Various types of AOPs have been successfully employed for the treatment of NAs in OSPW and showed promising results, including electro-oxidation (Abdalrhman & Gamal El-Din, 2020), photocatalysis (J. Liu et al., 2016; L. Meng et al., 2023; Suara et al., 2022), Fenton-based processes (Y. Zhang et al., 2016), ozonation (Gamal El-Din et al., 2011; Garcia-Garcia et al., 2011; Pereira et al., 2013; C. Wang et al., 2016), and sulfate-based processes (Fang et al., 2018; Song et al., 2022). While they offer the advantage of treating recalcitrant pollutants such as NAs, it is important to consider factors like reaction kinetics, energy consumption, and cost-effectiveness

when selecting the most appropriate AOP for a given application (Ayoub et al., 2010; S. Li et al., 2022; Parsons, 2015).

2.2 PMS Activation

PMS (CAS number 10058-23-8; molecular weight = 113.07 g mol^{-1} as HSO_5^-, and 614.74 g mol^{-1} as Oxone®) is a powerful oxidizing agent (see Table 2.1) that has gained significant attention recently for its application in water treatment (Anipsitakis & Dionysiou, 2003). The peroxymonosulfate anion (HSO_5^-) can be traced back to Caro's acid or peroxysulfuric acid (H_2SO_5), which was initially characterized by Heinrich Caro (Teixeira et al., 2013). Caro's acid is an extremely reactive acid that rapidly dissociates in water that has neutral pH values (e.g., OSPW) (Ghanbari & Moradi, 2017). Historically, stable mono-salts of Caro's acid have been challenging to be successfully synthesized (H. Sun & Wang, 2015; Teixeira et al., 2013). Consequently, PMS has been stabled in a triple salt ($2KHSO_5 \cdot KHSO_4 \cdot K_2SO_4$) marketed as Oxone® or Caroat, a white crystalline solid, non-toxic, cheap, and very soluble in water (>250 g L^{-1} at 20 °C) (Hussain et al., 2013). Furthermore, when compared to the conventional H_2O_2 solutions used in Fenton-based processes, Oxone® exhibits greater chemical stability, making it a good alternative for industrial uses due to being easier to handle during transportation and storage (Hussain et al., 2013). While PMS is a potent oxidizing agent, it possesses a slow direct reaction with organic contaminants in water, thus requiring activation. After activation, PMS is an electron acceptor and donor to generate radicals such as $SO_4^{\bullet-}$, $^{\bullet}OH$, and $O_2^{\bullet-}$ (Zhou et al., 2023). PMS activators can be classified into several primary categories, including transition metals, ultraviolet (UV) light, thermal energy (heat), ultrasound (US), electron conduction, and carbon-based catalysts (Ghanbari & Moradi, 2017; F. Meng et al., 2023; Saha et al., 2023; H. Sun et al., 2023; Xu et al., 2024; Zheng et al., 2022).

Specifically, some studies have used ozone, UV light, and iron oxide composite to activate PMS and degrade NAs species with degradation efficiencies over 80.0% (Fang et al., 2018; How et al., 2023; Song et al., 2022). Therefore, the oxidation potential and high degradation efficiencies obtained by PMS make it a valuable oxidant for OSPW treatment, contributing to the overall goal of reducing the environmental impact of oil sands companies operations.

2.3 Transitions Metals Biochar Composites

Recently, the use of metal-based catalysts for activating PMS has attracted growing interest because of their cost-efficiency, reduced energy demands, and the feasibility of upscaling in practical applications (R. Xiao et al., 2018; Zheng et al., 2022). Equations 2.1 and 2.2 describe the reaction produced when PMS is adsorbed on metal sites to generate $SO_4^{\bullet-}$ and $^{\bullet}OH$ species (Cao et al., 2019; Zheng et al., 2022; Zhou et al., 2023).

$$Me^n + HSO_5^- \rightarrow Me^{n+1} + SO_4^{\bullet-} + OH^- \quad (2.1)$$

$$Me^n + HSO_5^- \rightarrow Me^{n+1} + SO_4^{2-} + {}^{\bullet}OH \quad (2.2)$$

Nonetheless, the use of transition metal catalysts is often constrained by challenges such as leaching of metal ions and poor stability or agglomeration due to poor zeta potential values (S. Wang et al., 2019). Furthermore, certain transition metals, notably nickel and cobalt, pose a significant threat to public health. Their allergenic potential can result in adverse effects on the skin and airways. Moreover, their carcinogenicity is associated with their capability to penetrate cells through endocytosis, further emphasizing the potential risks they pose to human health (Egorova & Ananikov, 2017). Developing composite catalysts by loading environmentally compatible transition metals onto carriers represents a viable approach to address these limitations (H. Li et al., 2017). In particular, researchers are focusing on heterogeneous metal-based catalysts,

which involve solid catalysts that can be conveniently separated from the matrix for reuse, thereby preventing any potential secondary contamination linked to metal leaching (Oh et al., 2016; Oh & Lim, 2019).

In recent studies, researchers have extensively used biochar, a carbonaceous material produced through the pyrolysis of biomass under oxygen-deficient conditions, as a substrate or carrier for transition metal catalysts (Faheem et al., 2020; Lee & Park, 2020; X. Li et al., 2020; Premarathna et al., 2019). Specifically, the pyrolysis of biomass in oxygen-deficient conditions yields three primary products: the solid material named biochar, a liquid component called bio-oil, and syngas, which is a mixture containing carbon monoxide (CO), hydrogen (H_2), carbon dioxide (CO_2), and methane (CH_4) (Lehmann & Joseph, 2015). Biochar has emerged as an eco-friendly and cost-effective alternative for the elimination of both organic and inorganic pollutants through adsorption and AOPs when chemically modified for such purposes (Oliveira et al., 2017). Diverse sources of biomass, such as agricultural and forest residues, animal manure, sludge, and waste from food processing, have been utilized in the production of biochar (Medeiros et al., 2022). While the predominant element in biochar is carbon (C), it also contains hydrogen (H), oxygen (O), ash, and minor traces of nitrogen (N) and sulfur (S) (Jain & Khare, 2017). Moreover, the surface area and porous structure of biochar depend on the feedstock types and pyrolysis conditions, such as temperature and time (Mohammed et al., 2018). Biochar with high specific areas ensures the uniform distribution of transition metal catalysts, reducing their agglomeration, but also can provide electrons and accelerate the electron transfer in the catalytic reactions with oxidizing agents (G. Zhang et al., 2020). This approach has been proven effective in creating composite catalysts to activate PMS with exceptional efficiencies in water treatment (Álvarez et

al., 2020; Devi & Saroha, 2015; Pap et al., 2023; Peng et al., 2017; Y. Sun et al., 2019; J. Yan et al., 2015).

2.4 BC-Fe for PMS Activation

Iron, the fourth most predominant element in the crust of the Earth, has gained significant attention in research due to its environmentally friendly nature, cost-effectiveness, and superior reactivity compared to other transition metals. Among metal-based materials, iron species catalysts have been the central focus of investigation for activating PMS (Ghanbari & Moradi, 2017; Oh & Lim, 2019; J. Wang & Wang, 2018; Zheng et al., 2022).

In recent decades, there has been substantial research into the use of ZVI to mitigate the primary drawback of the Fe(II)/PMS system, which is the rapid consumption of ions during the treatment process (Cuervo Lumbaque et al., 2019; Oh & Lim, 2019; T. Zhang et al., 2020). ZVI is a promising catalyst due to its high reducibility (E^0 = -0.44 V), versability, and low toxicity (S. Xiao et al., 2020). Equations 2.3 to 2.7 describe the generation of radicals using a ZVI and PMS system (Cao et al., 2019; Ghanbari & Moradi, 2017; Rastogi et al., 2009; Tan et al., 2018; K.-S. Wang et al., 2010). Briefly, Fe^0 produces Fe(II) from the corrosion in the presence of H^+ and dissolved oxygen. (Equation 2.3). Then, Fe(II) is able to activate PMS, or the previously produced H_2O_2, to generate $^{\bullet}OH$ and $SO_4^{\bullet-}$ species (Equations 2.3, 2.5, and 2.6). As shown in Equation 2.7, previously produced Fe(III) can react with PMS to generate $SO_5^{\bullet-}$, which is a weak oxidant that can inefficiently degrade compounds compared to other generated radicals (Y. R. Wang & Chu, 2011). Additionally, high concentrations of ZVI and PMS may result in the scavenging of $SO_4^{\bullet-}$ and $^{\bullet}OH$ species, as shown in Equations 2.8-2.10 (Honarmandrad et al., 2023; Kusic et al., 2011; J. Wang & Wang, 2018). In this sense, the concentration of both ZVI and PMS are important factors that affect the performance of the system toward the degradation of the target contaminants.

$$Fe^0 + O_2 + 2H^+ \rightarrow Fe(II) + H_2O_2 \quad (2.3)$$

$$Fe(II) + HSO_5^- \rightarrow Fe(III) + SO_4^{\bullet-} + OH^- \quad (2.4)$$

$$Fe(II) + HSO_5^- \rightarrow Fe(III) + SO_4^{2-} + {}^{\bullet}OH \quad (2.5)$$

$$Fe(II) + H_2O_2 \rightarrow Fe(III) + {}^{\bullet}OH + OH^- \quad (2.6)$$

$$Fe(III) + HSO_5^- \rightarrow Fe(II) + SO_5^{\bullet-} + H^+ \quad (2.7)$$

$$Fe(II) + SO_4^{\bullet-} \rightarrow Fe(III) + SO_4^{2-} \quad (2.8)$$

$$HSO_5^- + SO_4^{\bullet-} \rightarrow SO_5^{\bullet-} + SO_4^{2-} + H^+ \quad (2.9)$$

$$HSO_5^- + {}^{\bullet}OH \rightarrow SO_5^{\bullet-} + H_2O \quad (2.10)$$

Numerous methods for fabricating ZVI particles have been documented in the literature. One of the simplest methods used for ZVI synthesis is the reductive precipitation of iron salts, a conventional wet chemical method (Khuntia et al., 2019). The colloidal behavior of these particles leads to a tendency for agglomeration (Phenrat et al., 2007). Consequently, contemporary approaches involve the utilization of water-soluble organic polymeric coatings, such as starch, sodium carboxymethyl cellulose, or pectin, to counteract agglomeration and improve stability (F. He & Zhao, 2007; Pardoe et al., 2001; Ponder et al., 2000). Additionally, carbonaceous materials have proven to be an excellent carrier for these particles (L. Chen et al., 2019; Y. Li et al., 2023; Peng et al., 2017; J. Wang et al., 2020). The immobilization of ZVI on the biochar substrate is a promising technology due to the high degradation efficiencies of organic compounds when used to activate PMS, low leaching tendency, easy separation due to magnetic properties, environmental compatibility, and cost-effectiveness.

CHAPTER 3 Experimental Method and Materials

3.1 Biomass and Chemicals

The raw OSPW utilized in this research was collected from an oil sands tailing pond located in Northern Alberta, Canada, and subsequently preserved in a cold storage room at 4 °C. The main properties of raw OSPW are listed in Table 3.1.

Table 3.1: Physicochemical characteristics of raw OSPW

Parameter		**Value**
pH		7.74±0.01
Conductivity (mS cm^{-1})		1.31±0.01
Dissolved organic carbon (DO; mg L^{-1})		5.78±0.04
Chemical oxygen demand (COD; mg L^{-1})		147.00±1.41
Dissolved organic carbon (DOC; mg L^{-1})		33.79±0.35
Turbidity (NTU)		15.74±1.05
Total suspended solids (TSS; mg L^{-1})		40.00±0.00
Total dissolved solids (TDS; mg L^{-1})		94.40±5.66
Total NAs (mg L^{-1})		15.76
Classical NAs	O_2-NAs (mg L^{-1})	8.78
Oxidized NAs	O_3-NAs (mg L^{-1})	4.23
	O_4-NAs (mg L^{-1})	2.47
	O_5-NAs (mg L^{-1})	0.17
	O_6-NAs (mg L^{-1})	0.12

Raw flax straw was used as feedstock for BC-Fe production and was provided by Inno Tech in Alberta, Canada. The following chemicals were used without any further purification: iron (III) chloride anhydrous ($FeCl_3$, 98.0%, Sigma-Aldrich, Germany), PMS (as triple salt $KHSO_5 \cdot 0.5KHSO_4 \cdot 0.5K_2SO_4$, 94.0%, Sigma-Aldrich, Switzerland), sodium sulfite (Na_2SO_3, 98%, Fisher Scientific, USA), DMPO (5,5-Dimethyl-1-pyrroline *N*-oxide, >99%, Dojindo Laboratories, Japan), BMPO (3,4-dihydro-2-methyl-1,1-dimethylethyl ester-2H-pyrrole-2-

carboxylic acid-1-oxide, >98%, Cayman Chemical, USA), analytical grade methanol (CH_3OH, 99.9%, Fisher Chemicals, USA), tert-butyl alcohol ($C_4H_{10}O$, 99.5%, Fisher Scientific, USA), and isopropyl alcohol (C_3H_8O, 99.8%, Fisher Chemicals, USA).

Before any experiment, OSPW samples were filtered using a vacuum filtration system equipped with a hydrophilic polycarbonate membrane of 8.0 µm pore size (TETP04700, Isopore™, Millipore, Germany). Ultra-pure water (Synergy UV, MilliporeSigma, USA) was used throughout the biochar composite production and solutions preparation. Pure nitrogen gas (N_2) (99%) was used in biochar and composite production.

3.2 Biochar Production

Collected flax straw (Figure 3.1a) was washed with ultrapure water to remove the impurities and then dried in an oven (Fisherbrand™ Isotemp™, Fisher Scientific, USA) at 105 °C overnight. The biomass was crushed with a porcelain mortar and pester, screened through a sieve to collect particles of size smaller than 1.4 mm, and stored in air-tight glass containers.

The pristine or unmodified biochar (Figure 3.1b), FL600, was obtained from raw flax straw through pyrolysis under N_2 environment using a muffle furnace (Lindberg Blue M, Thermo Scientific™, USA). Based on previous studies, a pyrolysis temperature of 600 °C was selected to prepare the materials (Song et al., 2022) under the following conditions: 10 °C min^{-1} of heating rate until reaches 600 °C, maintaining that temperature for 2 h, and cooling the system to approximately 80-100 °C. In all synthesis steps, 99% pure N_2 was supplied at 2 L min^{-1}. The pristine biochar was labeled as FL600 and stored in air-tight glass containers for control experiments.

The BC-Fe composite (Figure 3.1c) was produced by adding 5 g of raw flax straw into a flask containing 100 mL of a 0.1 M $FeCl_3$ solution. Flasks were covered and placed in a platform

shaker (New Brunswick™ Innova® 2100 platform shaker, Eppendorf Inc., USA) at 200 rpm for 60 min. Then, the water in the mixture was partly evaporated using a magnetic stirrer at 80 °C for 2 h. Subsequently, the samples were put in the oven at 105 °C overnight. Pyrolysis was performed in a muffle furnace at conditions listed previously at 600 °C for 2 h. The products were grounded using a porcelain mortar and pester, sieved through a 425 µm mesh. Finally, the Fe-based composite was labeled as FL600-Fe and stored in air-tight glass containers for later use.

(a) **(b)** **(c)**

Figure 3.1: (a) Raw flax straw, (b) Pristine flax straw biochar (FL600), and (c) FL600-Fe.

3.3 Characterization of Biomass, Pristine Biochar, and Modified Biochar

3.3.1 Surface Area and Porous Properties

The specific area, pore volumes, and pore sizes were measured using a high vacuum physisorption/chemisorption analyzer (Autosorb-iQ, Quantachrome, USA). The samples were outgassed before N_2 adsorption at 350 °C for 4 h. The specific surface area (S_{BET}) and the total pore volume (V_{TOT}) of the samples were determined using the Brunauer, Emmett, and Teller (BET) method.

3.3.2 Zeta Potential

The particle stability in terms of zeta potential was determined using a particle size and zeta potential analyzer (NanoBrook Omni, Brookhaven Instruments Corporation) that utilizes the Phase Analysis Light Scattering (PALS) method with a detection range of -500 mV to 500 mV and a mobility range of 10^{-11} to 10^{-7} $m^2/V•s$.

3.3.3 Point of Zero Charge

Point of zero charge (pH_{pzc}) was determined based on the salt addition method previously described in detail by Nguyen et al. (2022) and Jang et al. (2018). Briefly, the pH of a 0.01 M NaCl solution was adjusted using a 0.1 M solution of HCl or a 0.1 M solution of NaOH to the pH range from 2 to 10. Once the pH (initial pH = pH_o) was adjusted, 5 mg of the composite was added to falcon tubes containing 25 mL of the 0.01 M NaCl solution. The tube was filled with nitrogen gas to minimize the CO_2 effect in the head space. The falcon tubes were sealed and placed on a platform shaker at 150 rpm for 48 h. After the agitation period is completed, the equilibrium pH (final pH = pH_f) will be recorded. For each container, the difference between the pH (ΔpH) values was calculated by the subtraction of pH_o to the pH_f. Then, ΔpH vs. pH_o was plotted, and pH_{pzc} was determined when $\Delta pH = 0$.

3.3.3 Field Emission Scanning Electron Microscopy (FESEM)

The surface morphology of the samples was examined by employing a field emission scanning electron microscopy paired with an energy-dispersive X-ray spectrometer (FESEM-EDX, Zeiss Sigma, Germany) at 10.00 kV. The magnification values used were 2.50 Kx, 5.00 Kx, and 10.00 Kx. Before FESEM analysis, samples were sputtered with a 16 nm layer of gold to enhance the clarity and quality of the images.

3.3.4 Surface Functional Groups

Fourier transform infrared (FTIR) spectroscopy (Nicolet™ 8700 FTIR Spectrometer and Continuum™ FTIR Microscope, Thermo Scientific, USA) analysis was conducted to assess the functional groups in the surface between 400 and 4000 cm^{-1} at 4 cm^{-1} resolution. Before FTIR analysis, samples were compacted into KBr pellets.

3.3.5 Crystallographic Structures

The X-ray diffraction (XRD) analysis was performed to determine the crystallographic properties of the samples using an X-ray diffractometer (Ultima IV, Rigaku, Japan) at a scanning rate of 2° min^{-1} between 5 and 90° 2θ angles with a cobalt tube at 38 kV and 38 mA.

3.3.6 Elemental Distribution

X-ray photoelectron spectroscopy (XPS, Kratos AXIS Ultra, Kratos Analytical, UK) was used to obtain the surface chemical composition and chemical states of the raw flax straw, unmodified biochar, and composite before and after removal.

3.3.7 Thermostability and Proximate Analysis

The thermostability of the materials was determined using a thermogravimetric analyzer (Pyris 1 TGA, Perkin Elmer, USA) between 105 and 900 °C at a heating rate of 20 °C min^{-1} with N_2 as a purge gas. Proximate analysis was performed based on the method described by Crombie et al. (2013) to determine moisture, volatile matter, ash, and fixed carbon content by weight loss.

3.3.8 Ultimate Analysis

The carbon (C), hydrogen (H), nitrogen (N), and sulfur (S) percentages in the samples were determined using an elemental analyzer (Flash 2000 CHNS/O analyzer, Thermo Scientific, USA).

The oxygen concentration was estimated by difference (100 – C(%) – H(%) – N(%) – S(%) – Ash(%)) on a dry-mass basis.

3.3.9 Magnetic Properties

The magnetic properties in the modified biochar were measured using a Superconducting quantum interference vibrating sample magnetometer (SQUID VSM, Quantum Design MPMS®3, Quantum Design, USA) at an operating temperature range of 25 °C and a magnetic field range of -40 kOe to +40 kOe.

3.4 Degradation Experiments Using FL600-Fe and PMS for NAs Removal

3.4.1 Experimental Setup and Analytical Procedures

Removal experiments were conducted in 125 mL Erlenmeyer flasks containing the composite catalyst and OSPW, which were then covered with parafilm and positioned on a platform shaker (New Brunswick™ Innova® 2100 platform shaker, Eppendorf Inc., USA) at an agitation of 200 rpm at room temperature (25±2 °C). After reaching the adsorption equilibrium, based on the adsorption of fluorophore organic compounds, a predetermined dose of PMS was added to initiate the AOP treatment of OSPW. After the completion of contact time, samples were collected from the system and filtered with 0.2 µm syringe filters (Basix™ Nylon Syringe Filters, Fisher Scientific, USA) to separate the composite from treated OSPW. Samples were quenched to avoid chemical oxidation by residual PMS using a corresponding volume of 1 M sodium sulfite solution for the adsorption equilibrium experiments and methanol for NAs removal experiments. Samples were stored at 4 °C until analysis.

The adsorption equilibrium of FL600-Fe was determined through synchronous fluorescence spectroscopy (SFS) using a fluorescence spectrophotometer (Cary Eclipse, Varian,

Germany) as a semi-quantitative analysis to detect fluorophore organic compounds in OSPW, including some NAs. The spectrophotometer was set at a scanning speed of 600 nm min^{-1}, a photomultiplier voltage of 800 V, and fixed excitation (200-600 nm) and emission (218-618 nm) wavelength ranges.

Ultra-high performance liquid chromatography-quadrupole time-of-flight mass spectrometry (UPLC-QTOF-MS, Synapt G2, Waters™, USA) with electrospray ionization (ESI) in negative mode and equipped with a BEH Phenyl column (150 mm×1 mm, 1.7 μm particle size) was utilized to measure the NAs concentration in the raw and treated OSPW through chromatographic separations and using myristic acid-1-^{13}C as an internal standard.

3.4.2 Adsorption Equilibrium Experiments

Initially, experiments were performed to obtain the adsorption equilibrium of fluorophore compounds using solely FL600-Fe in OSPW. Briefly, 1 g L^{-1} of the composite was added into an OSPW solution, and the mixture was then agitated for 15, 30, 45, 60, and 120 min to determine when the adsorption equilibrium of fluorophore organic compounds in OSPW was reached. This point of time was then used to begin the catalytic PMS activation process for NAs degradation.

3.4.3 Kinetic Experiments

The effect of the catalyst and the oxidant dose were studied to evaluate the optimal concentrations for NAs removal in real OSPW. The catalyst composite was added into an OSPW solution at different concentrations (0.25, 0.5, 1, and 2 g L^{-1}) in an Erlenmeyer flask under agitation. After completing adsorption equilibrium, a specific dose of PMS (0.25, 0.5, 1, and 2 mM) was added to the mixture to initiate the reaction. At pre-determined time intervals, 250 μL of the filtered solution was withdrawn and immediately quenched by 250 μL of methanol to stop residual PMS. Samples were stored at 4 °C to be analyzed by the UPLC-QTOF-MS equipment.

Next, the most effective dose of FL600-Fe and PMS was identified for use in subsequent experiments. Control experiments were performed using pristine biochar, engineered biochar, and PMS solely in OSPW.

3.4.4 Oxidant Consumption

PMS consumption in the system was determined using a spectrophotometer at 530 nm (Ultrospec 2100 pro, Biochrom) by the *N,N*-diethyl-p-phenylenediamine (DPD) method at time intervals from 0 to 120 minutes of reaction after adsorption equilibrium. Samples were withdrawn from the solution and filtered with 0.45 µm syringe filters (Basix™ Nylon Syringe Filters, Fisher Scientific, USA) before analysis.

3.4.5 Role of Reactive Radicals in the FL600-Fe/PMS System

Scavenger experiments and EPR measurements were conducted to identify the main reactive oxygen species generated in the application of the FL600-Fe/PMS system under the best experimental conditions.

(i) Quenching experiments: the contribution of the potential oxidizing species $^{\bullet}OH$ and $SO_4^{\bullet-}$ was studied in the FL600-Fe/PMS system in removing NAs from real OSPW. Scavenger experiments were performed by adding a 0.4 M solution of isopropyl alcohol (IPA) or tert-Butyl alcohol (TBA) to the reaction mixture. TBA is an effective quencher for $^{\bullet}OH$, whereas IPA is capable of scavenging both $^{\bullet}OH$ and $SO_4^{\bullet-}$ (L. Gao et al., 2022). Initial and final samples (120 min contact time after adsorption equilibrium) were withdrawn from the solution and filtered with 0.2 µm syringe filters (Basix™ Nylon Syringe Filters, Fisher Scientific, USA). Samples were stored at 4 °C before UPLC-QTOF-MS analysis.

(ii) EPR measurements: main radical species generated during OSPW treatment using the FL600-Fe/PMS system were identified using EPR spectroscopy (Elexsys E−500 spectrometer,

Bruker, USA) with a center field of 3505 G, sweep width of 100 G, field modulation of 1 G, microwave frequency of 9.8 GHz, microwave power of 20 mW, and sweep time of 120 s. The treatment of OSPW took place in 10 mL beakers containing a 50 mM DMPO solution for detecting $^{\bullet}OH$ and $SO_4^{\bullet-}$, and a 50 mM BMPO solution for detecting $O_2^{\bullet-}$ and $^{\bullet}OH$. After brief agitation, the reaction solution was transferred into 50 μL micro-capillary tubes and inserted into a 3 mm ESR tube, which was then placed in the resonator. Control experiments were performed using solely FL600-Fe, PMS, and raw OSPW.

3.4.6 Leaching Study

The leaching of iron from Fe-loaded biochar could pose a potential concern of residual contamination when using these materials for water treatment. Hence, a leaching study was performed to determine if iron from the composite might be released into the OSPW during treatment. The iron leaching concentration for each material in OSPW was measured using Inductively Coupled Plasma-Atomic Emission Spectrometry (Thermo iCAP6300 Duo ICP-OES, Thermo Fisher Scientific, UK) according to the EPA Method 6010D. The concentration of iron ions was determined for raw OSPW, treated OSPW using 1 g L^{-1} of FL600-Fe solely at 45 min contact time, and treated OSPW using FL600-Fe/PMS at 120 min contact time with PMS after adsorption equilibrium time. After the completion of contact time, samples were filtered with 0.2 μm syringe filters (Basix™ Nylon Syringe Filters, Fisher Scientific, USA).

3.4.7 Microbial Viability Assay

A microbial viability assay using 21 h of exposure to untreated and treated OSPW was performed to investigate the impact of the proposed treatment on bacterial growth and survival. This method employed *Staphylococcus warneri* bacteria (NCTC 5955) and followed the established clinical practice for dilution of antimicrobial tests for aerobic bacteria (Clinical and

Laboratory Standards Institute, 2018). Briefly, tryptic soy agar (TSA) was used to incubate *Staphylococcus warneri* at 37 °C for 24 h. A single colony was isolated from the primary culture to generate a secondary culture in each replicate, maintaining the same incubation conditions. This secondary culture was employed to prepare a bacterial suspension in 0.9% NaCl. Samples were diluted at 90% (*V*/*V*) with tryptic soy broth (TSB) and inoculated with an initial cell density of 6.0±0.5 Log colony forming units (CFU) per mL. Subsequently, 180 µL of the positive control (30 mg L^{-1} of phenol), untreated, and treated OSPW samples were loaded into a 96-well plate in triplicates. The exposure time started when 20 µL of the bacterial culture was introduced to wells, and sterility controls were performed on the same plate by adding 20 µL of TSB to OSPW samples and the positive control. After the completion of the incubation time, 100 µL from each well was diluted from 10^0 to 10^8 CFU mL^{-1} in 0.9% NaCl and then placed for a 21 h of incubation on TSA. Finally, the colonies were counted to determine the microbial viability. A two-tailed distribution and homoscedastic variation t-test were used for data analysis and positive control comparison. Furthermore, the notation ** represents a significance level of $P<0.01$.

3.4.8 Quantification of Bioavailable Acid Extractable Organics (AEOs)

Biomimetic extraction through solid phase microextraction (BE-SPME) was employed to assess the bioavailability of AEOs that can contribute to toxicity in both untreated and treated OSPW. This technique quantifies bioavailable AEOs in OSPW, including NAs and dissolved hydrocarbons for both neutral and ionizable organics. This procedure had been previously explained and examined by Redman et al. (2018). OSPW samples were acidified using 50 µL of phosphoric acid to reduce the pH to 2.4 in 20 mL glass vials and then placed in the SPME autosampler. Subsequently, 30 µm of polydimethylsiloxane (PDMS) SPME fibers were added for equilibration, and samples were under orbital agitation (250 rpm) at 30 °C for 100 min. Once the

equilibration/extraction phase was finished, the fiber was retracted and introduced into the injection port at 300 °C on the gas chromatograph equipped with a flame ionization detector (Autosystem XL GC System with FID, PerkinElmer, USA) at a rate of 45 °C min^{-1}. Then, the fiber underwent a thermal desorption process for 3 min to desorb the organic components that had been partitioned to the PDMS. The BE-SPME results were then in terms of μmol of 2,3-dimethylnaphthalene (2,3- DMN) per mL of PDMS.

3.4.9 Regeneration and Reuse of Spent Composite

The spent FL600-Fe was obtained after treatment experiments using a composite concentration of 1 g L^{-1}, a PMS dose of 1 mM, and a contact time of 2 h with real OSPW. The spent biochar was dried at 105 °C overnight prior to regeneration through thermal pyrolysis at 600 °C for 2 h under N_2 atmosphere. The regenerated biochar was applied in the degradation of NAs from real OSPW at the same doses and contact time used in the initial experiment. All experiments were performed in duplicate. One cycle was respective of one spent biochar regeneration and one treatment experiment using regenerated biochar. A total of four consecutive cycles were performed to determine the efficiency of biochar reusability.

CHAPTER 4 Results and Discussion

4.1 Characterization of Biochar

4.1.1 Yield, Surface Area, and Porous Properties

The biochar yield, surface area, and porous properties of the pristine biochar and composite are presented in Table 4.1. Biochar yield refers to the percentage of the solid fraction obtained by pyrolysis and depends directly on the composition of the feedstock, type of modification, and pyrolysis temperature (L. Zhao et al., 2013). Typically, the biochar yield from agricultural waste biomass ranges from 30 to 60% (Hai et al., 2023). The composite has a higher yield than the pristine biochar, indicating higher conversion of the modified feedstock into a solid product due to the substitution of the weight content of volatile organics with iron. The composite had a surface area of 117.82 m^2 g^{-1} and a pore volume of 0.43 cm^3 g^{-1}, which were 2.68 and 5.38 times higher than the pristine biochar. According to Song et al. (2022), the iron particles attached to the surface of the nanocarrier increased the surface area of the catalyst and may increase the number of available adsorbent sites for the NAs to attach compared to the pristine biochar (Song et al., 2022).

Table 4.1: Surface area and porous properties of raw flax straw, pristine biochar (FL600), and FL600-Fe.

Properties	**FL600**	**FL600-Fe**
Yield (%)	30.32	47.61
Surface area (m^2 g^{-1})	43.95	117.82
Total Pore Volume (cm^3 g^{-1})	0.08	0.43
Average pore radius (nm)	32.35	6.81

4.1.2 Zeta Potential

The stability of FL600 and FL600-Fe was measured using zeta potential analysis in solution at neutral pH. When the absolute zeta potential value is high, the stability of the dispersed system improves (Ma et al., 2023). Values above |30| mV are optimal for full electrostatic stabilization, in which electric repulsion occurs and there is less particle aggregation (Heurtault, 2003). The FL600-Fe composite has a zeta potential of 43.36±1.03 mV, while the pristine FL600 has a zeta potential of -39.18±7.14 mV. These values suggest that both materials are above the optimal value to avoid the flocculation of particles and are stable. The zeta potential value of the pristine biochar reflects that the surface is negatively charged, and after modification with $FeCl_3$, the surface of the composite biochar becomes positive. In this sense, as PMS (HSO_5^-) is an anion, the electrostatic interaction between the composite and the oxidant is expected to be high, improving the activation process and consequently, the generation of radicals in this system (Silvestri et al., 2020).

4.1.3 Point of Zero Charge

The pH_{pzc} of FL600 and FL600-Fe was determined using the salt addition method (Jang et al., 2018; Nguyen et al., 2022). The pH_{pzc} of the unmodified biochar was determined to be 9 (Figure 4.1), where the ΔpH is equal to 0. In contrast, the pH_{pzc} of the composite is 2, which is significantly lower than the value of the pristine biochar. At a pH matching the pH_{pzc}, electrostatic interactions play a key role in the adsorption process. However, if the pH surpasses the specified pH_{pzc}, there might be electrostatic repulsion instead (W. Chen et al., 2017). Based on the results, FL600-Fe is less likely to adsorb NAs from OSPW due to electrostatic repulsion than FL600, since the matrix has a pH of 7.7. Nevertheless, besides the point of zero charge, other factors may influence the adsorption capacity of materials, such as the surface area and functional groups. The results in

section 4.3.3 showed that the composite exhibited a slightly superior adsorption performance compared to the pristine biochar. This improvement can be primarily attributed to its increased surface area, providing a greater number of adsorption sites for contaminants to attach to. In general, both materials demonstrated a constrained adsorption capacity. However, it is essential to emphasize that the primary focus of this study was the degradation of NAs through an AOP treatment. This removal was achieved through the activation of PMS utilizing ZVI particles on the surface, rather than relying on the adsorption of these pollutants.

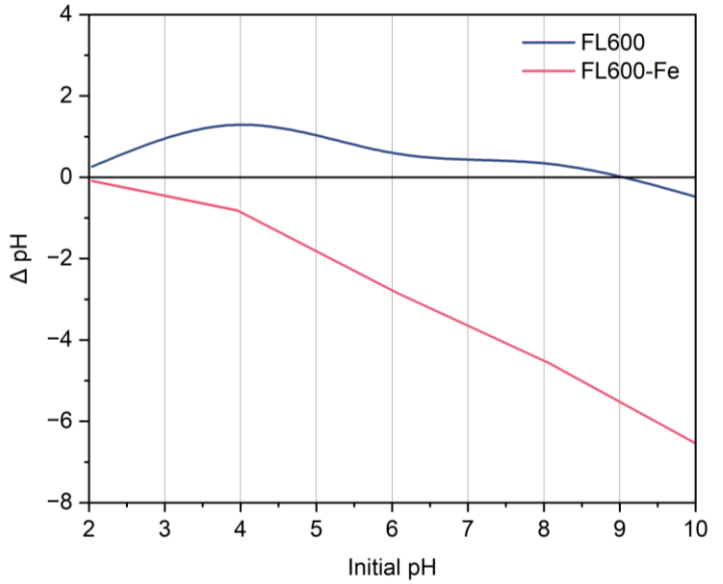

Figure 4.1: Point of zero charge for FL600 and FL600-Fe.

4.1.4 Field Emission Scanning Electron Microscopy (FESEM)

Cellulose fibers were observed in the FESEM images of the raw flax straw material (Figure 4.2a), and this is confirmed by the XRD results (see subsection 4.1.5). When pyrolyzed to FL600 (Figure 4.2b), the unmodified material showed a lack of roughness correlated to the low surface area, indicating a low adsorption capacity. Nevertheless, porous properties are reflected in the images, suggesting a potential for good retention and attachment for modification material inside

the pores of the biochar. When activated with $FeCl_3$ (Figure 4.2c), the FESEM results show that the existing pores of the unmodified biochar were filled by iron as well as particle attachment to the surface of the support carrier. This analysis aligns with the presence of iron observed using XRD and the presence of Fe2p displayed in the XPS survey scan (shown in subsection 4.1.6), supporting a successful incorporation of the modification. This pattern was also reported by Hasan et al. (2021), in which high porosity and smooth surface in unmodified biochar led to an effective agglomeration of iron particles within the composite material.

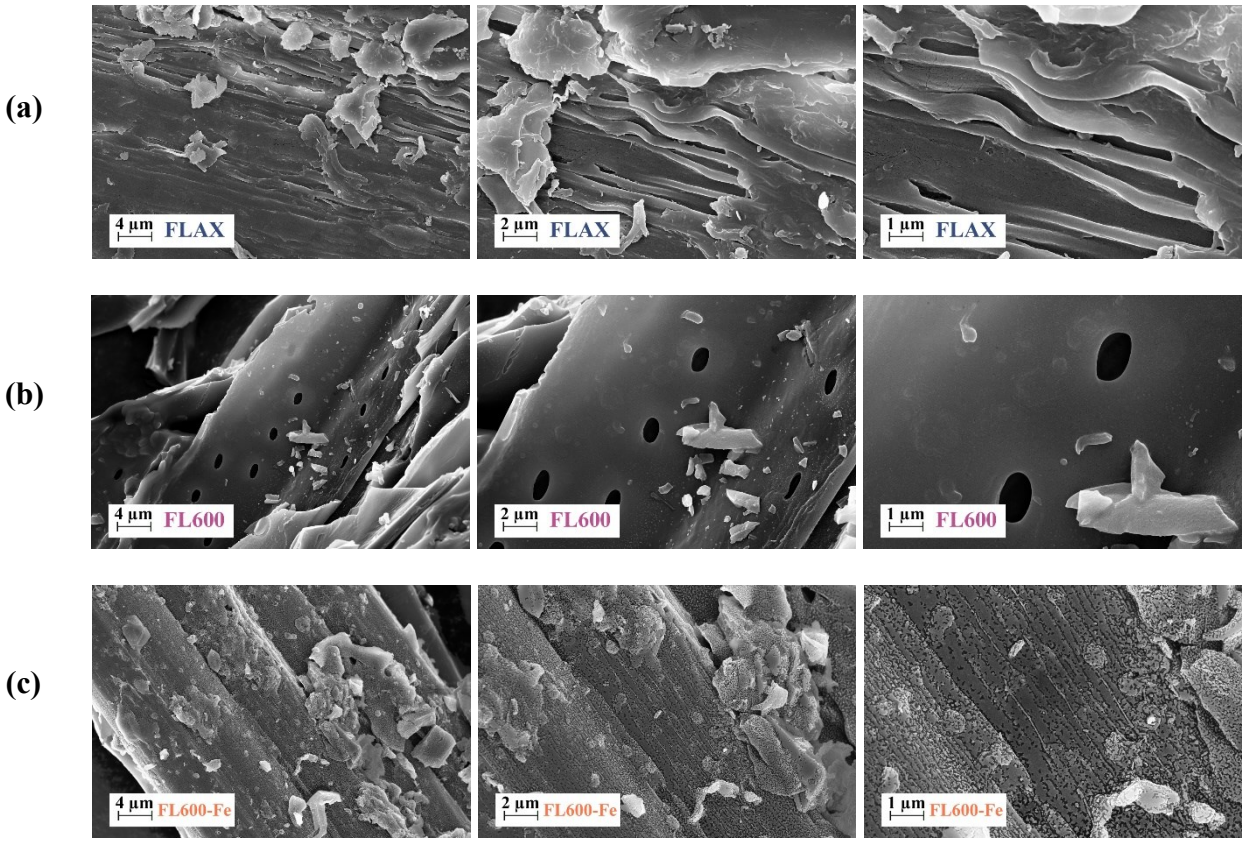

Figure 4.2: FESEM images at 2.5 Kx, 5 Kx, and 10 Kx magnification of (a) raw flax straw, (b) pristine biochar FL600, and (c) FL600-Fe.

4.1.5 Surface Functional Groups

The FTIR spectra of the raw material, pristine biochar, and the composite pre- and post-treatment are presented in Figure 4.3. This technique is able to show changes in the functional groups on the surface of the material when pyrolyzed from flax straw into biochar, but also possesses the capability to distinguish minor differences between biochar pre- and post-modification that would not be noticed visually (Chia et al., 2012; Hamid et al., 2022). All samples display common band lengths of –OH stretching (3450 cm^{-1}, presence of alcohol), C–H stretching (2925 and 2850 cm^{-1}, presence of alkane groups), C=C stretching (1625 cm^{-1}, conjugated alkene), C–O stretching (1080 cm^{-1}, primary alcohol), and C–H bending vibrations or CH deformation (wavenumber below 800 cm^{-1}, including peaks at 615 and 465 cm^{-1}) (Chia et al., 2012; Y. Liu et al., 2015).

Based on the spectrum, the bands displayed at 2925 and 2850 cm^{-1} are associated with symmetric stretching of C–H vibrations and could indicate the presence of organic contaminants (Russell & Fraser, 1994). Since both peaks decreased their intensity after pyrolysis, these compounds were partially degraded from the raw material, as confirmed by the first derivative of thermogravimetric analysis (DTG) curves. Additionally, it can be observed that the intensity of the peaks for the band range of 1600-800 cm^{-1} decreased with the pyrolysis of the material, suggesting ignition loss of –OH and C–H content, which correlates with the reduction in hydrogen content in the ultimate analysis. The increase in the absorbance peak after treatment observed at the band 1080 cm^{-1} (associated with C–O stretching) indicated the presence of carboxylic groups in the floc, thus confirming the presence of a portion of NAs adsorbed in the samples from OSPW (Wan et al., 2019).

Yan et al. (2013) and Y. Sun et al. (2019) suggested that the peak for Fe–O complexes and/or iron oxides on the composites is usually found at the 680 cm^{-1} band when Fe^{3+} hydrolysis occurs after $FeCl_3$ pretreatment (Devi & Saroha, 2015; Y. Sun et al., 2019). In the present study, these peaks are not found on the composite FTIR spectra, suggesting that the product of $FeCl_3$ transformation through pyrolysis is ZVI or Fe^0, as confirmed by the XRD analysis (next subsection). On the other hand, a C-Cl vibration mode peak at band 465 cm^{-1} can be found after $FeCl_3$ modification (A. L. Gao & Wan, 2023).

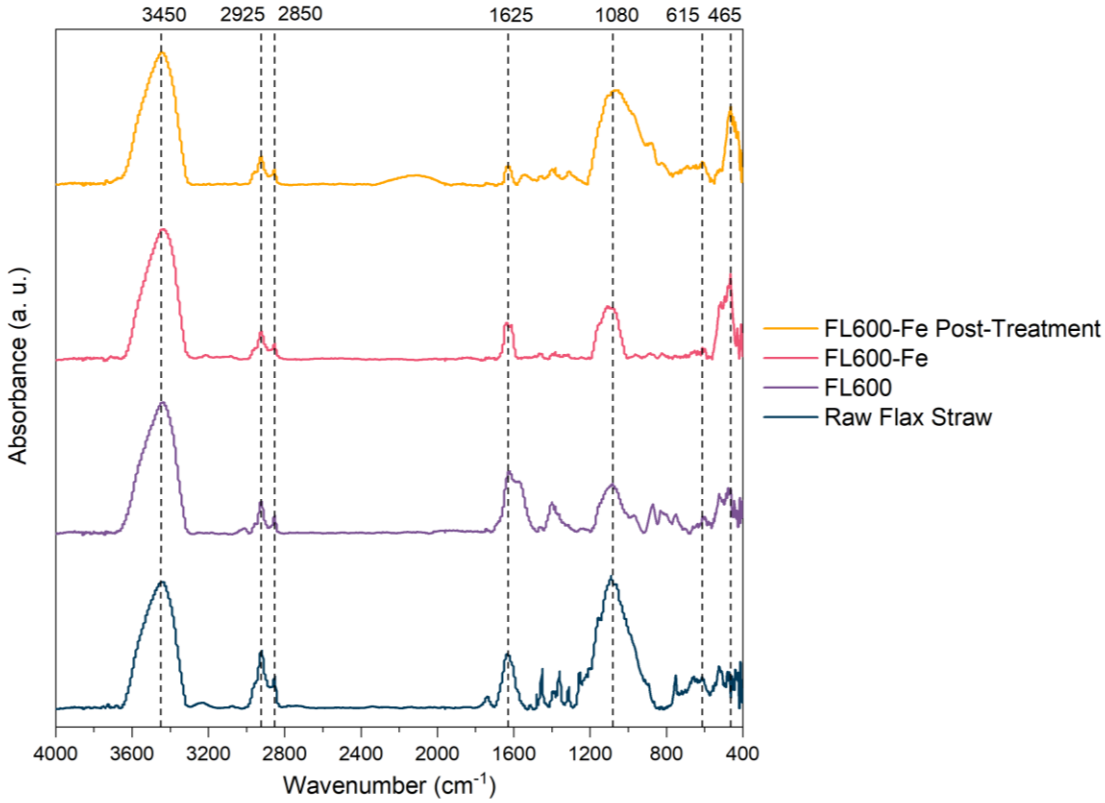

Figure 4.3: FTIR spectra of raw flax straw, pristine biochar (FL600), and FL600-Fe pre- and post-treatment.

4.1.6 Crystallographic Structures

The XRD analysis was performed to determine the crystalline phases on the feedstock, pristine biochar, and composite, and the patterns are shown in Figure 4.4. Flax straw has cellulose crystalline microfibrils that provide the main support for a core of amorphous polysaccharides, such as hemicelluloses, pectins, and lignin (C. Chen et al., 2020; Richely et al., 2022). This component is confirmed by the diffractogram for flax straw, in which the presence of cellulose is observed in the peaks at 2θ of 17.30, 19.15, and 26.22°. After the pyrolysis process, pyrrhotite, kalicinite, ankerite, calcium carbonate, and quartz microcrystals appeared in the XRD pattern, as well as the peaks for cellulose content.

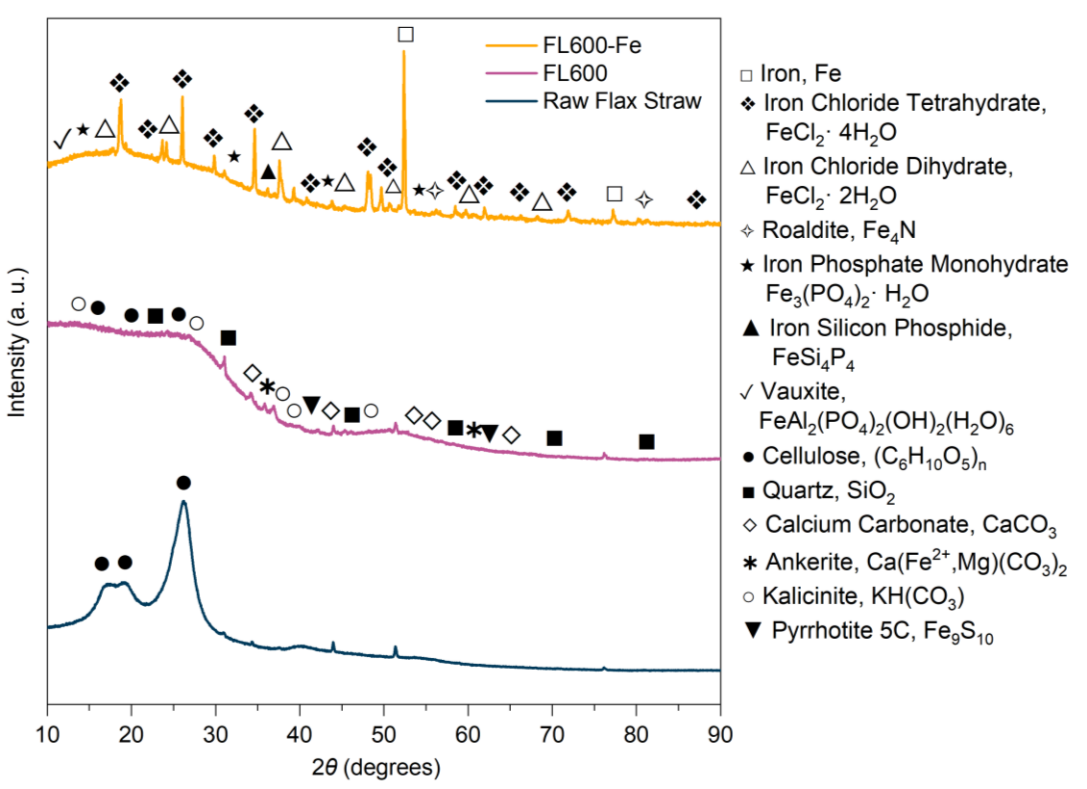

Figure 4.4: XRD diffractograms of raw flax straw, pristine biochar (FL600), and FL600-Fe.

4.1.7 Elemental Distribution

The surface chemical composition and chemical states of the raw flax straw, pristine biochar, the composite, and the composite after treatment were assessed using XPS analysis. The survey spectra for these materials can be found in Figure 4.5.

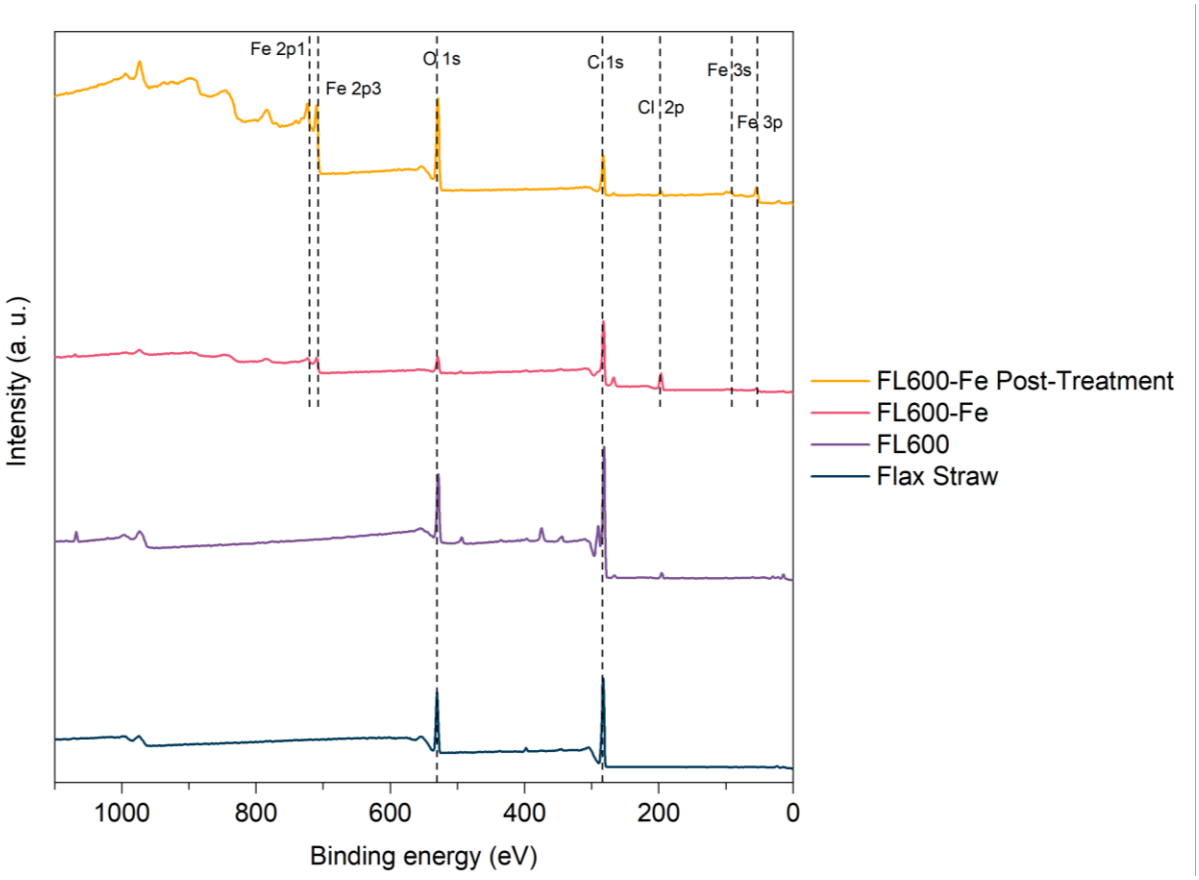

Figure 4.5: XPS survey spectra of raw flax straw, pristine biochar (FL600), FL600-Fe, and FL600-Fe collected post-treatment.

The four materials present C 1s (284.50 eV) and O 1s (531.88 eV) peaks (Vincent Crist, 2018). After pyrolysis of flax straw, the pristine biochar shows an increase of C 1s peak intensity, suggesting the increase of carbonaceous material (Morgan, 2021). On the other hand, the FL600-Fe composite presents a lower peak than the unmodified material due to an increasing iron conversion. This behavior is corroborated by elemental composition analysis, in which the order

of carbon content is described as follows: Flax Straw < FL600-Fe < FL600. Interestingly, the O 1s peak of FL600-Fe increased after treatment, suggesting that adsorption onto oxygen-containing functional groups may have been achieved through hydrogen bonding and hydrophobic interaction (Inyang & Dickenson, 2017; Song et al., 2022).

Five new peaks appear after $FeCl_3$-modification of the biomass. The iron content can be observed on the Fe 2p3 (707 eV) and Fe 2p1 (720 eV) predominant peaks (Vincent Crist, 2018). Additionally, small peaks corresponding to Fe 3s (91.50 eV) and Fe 3p (53 eV) can be described on the survey spectra of FL600-Fe (Song et al., 2022; Vincent Crist, 2018). The presence of this modification can be confirmed by previous XRD analysis and FTIR spectra. On the other hand, chlorine groups were also observed after modification as Cl 2p (198.08 eV) peaks (Vincent Crist, 2018). FTIR spectra confirmed a C-Cl vibration mode peak and two crystalline phases containing Cl were also observed in XRD analysis (A. L. Gao & Wan, 2023).

The deconvolution peaks of carbon and oxygen can be observed in Figures 4.6 and 4.7. The deconvoluted O 1s XPS spectra showed three peaks for flax straw, FL600, FL600-Fe, and FL600-Fe post-treatment at are assigned to C-O and C=O (dos Reis et al., 2022; Jieying Zheng et al., 2014). The ketonic functional group (-C=O), with its lone-pair electrons acting as Lewis basic sites, forms strong bonds with PMS. This interaction results in the transfer of an electron to PMS, causing the cleavage of the O-O bond and the generation of active radicals, specifically $SO_4^{\bullet-}$ and $^{\bullet}OH$ (Huong et al., 2020). The increase in the absorbance peak associated with C–O and the decrease of C=O indicated the presence of carboxylic groups in the floc, thus confirming the presence of a portion of NAs adsorbed in the samples from OSPW as also confirmed by FTIR (Wan et al., 2019). The deconvoluted C 1s XPS spectra showed three peaks for flax straw, FL600, FL600-Fe, and FL600-Fe post-treatment are assigned to C=O, C–OH, and C=O (Cho et al., 2021).

These peaks confirm the presence of carboxylic groups in surface of the composite (Cui et al., 2014; Shen et al., 2020).

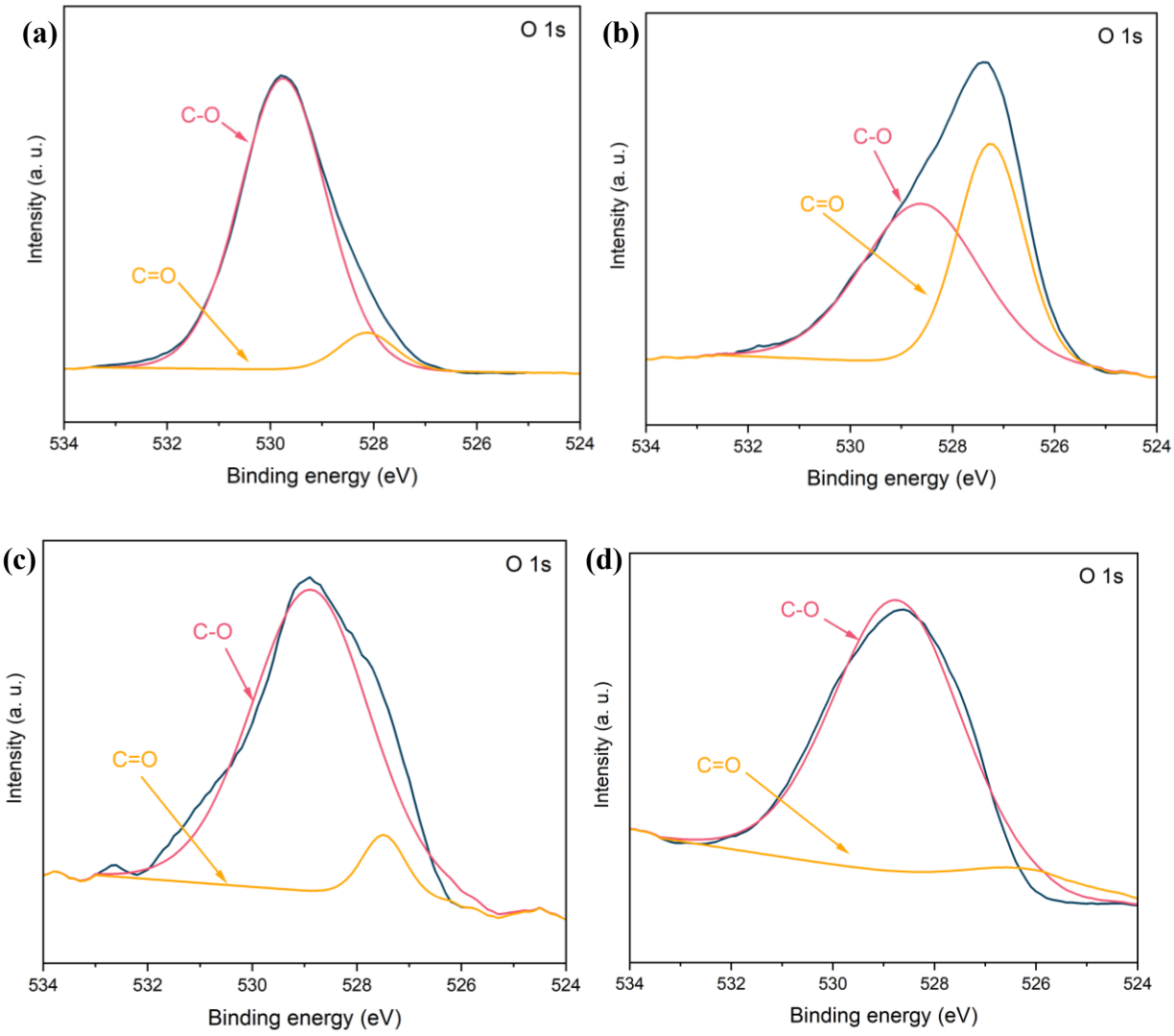

Figure 4.6: Deconvoluted O 1s XPS spectra of (a) raw flax straw, (b) pristine biochar (FL600), (c) FL600-Fe, and (d) FL600-Fe collected post-treatment.

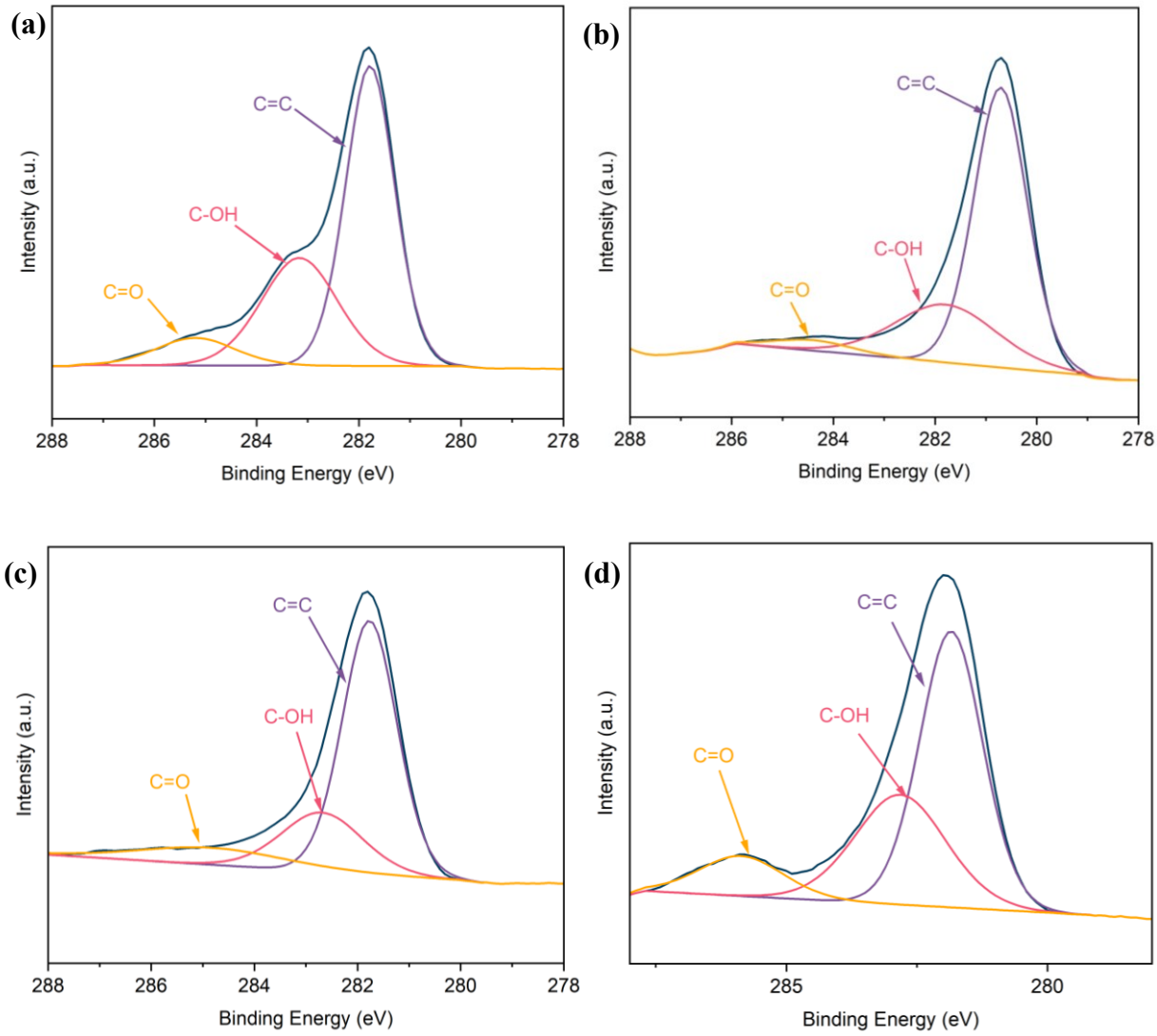

Figure 4.7: Deconvoluted C 1s XPS spectra of (a) raw flax straw, (b) pristine biochar (FL600), (c) FL600-Fe, and (d) FL600-Fe collected post-treatment.

4.1.8 Thermostability, Proximate Analysis, and Ultimate Analysis

The thermostability of the raw flax straw, pristine biochar, and the composite was evaluated, and the mass loss results are shown in Figure 4.8. These outcomes were used to determine the moisture, volatile matter, ash, and fixed carbon content (Table 4.2). Usually, the TGA/DTG curve can be divided into four distinct regions. The first region corresponds to the mass loss related to moisture evaporation ($0 \leq T \leq 200$ °C). In the second region, the breakdown of

carbohydrates is displayed (200 ≤ T ≤ 600 °C) (Fan et al., 2018; Hernandez-Mena et al., 2014). The third region indicates the degradation of aromatic compounds (600 ≤ T ≤ 800 °C) (Ghodke et al., 2021; Nzediegwu, Arshad, et al., 2021), and finally, the fourth region illustrates the decomposition of inorganic components and thermally stable compounds (T ≥ 800 °C) (Fan et al., 2018; Hernandez-Mena et al., 2014).

As shown in Figure 4.8a the thermostability of the pristine and modified biochar greatly increased after pyrolysis since thermal decompaction occurs at much higher temperatures (550 °C) compared to flax straw (200 °C). The weight loss was 77.03, 13.26, and 29.01% for flax straw, FL600 and FL600-Fe, respectively. The thermal decomposition process is nearly finished at 750 °C for the pristine and composite biochar and is considered relatively stable, with a subsequent mass loss of only 3.82 and 7.22%, respectively. Furthermore, it can be inferred from the TGA curve that the pyrolysis zone for the raw flax occurred within the temperature range of 200 – 600 °C.

The differential thermogravimetry (DTG) graph shown in Figure 4.8b is a helpful analysis for assessing the thermal degradation pathways of the feedstock (Nzediegwu, Naeth, et al., 2021). This analysis revealed a significant degradation stage occurring between 250 and 550 °C, signaling the decomposition of volatile and organic compounds within the flax straw (Jerez et al., 2021; Xia et al., 2016), and contents of cellulose previously identified in the XRD analysis (Nzediegwu, Arshad, et al., 2021). The pristine and modified biochar did not show this degradation step due to the degradation of these compounds due to previous pyrolysis at 600 °C. Additionally, the DTG curve for FL600-Fe presents a weight loss peak at 600–800 °C, indicating the degradation of large molecules of aromatic compounds (Nzediegwu, Arshad, et al., 2021).

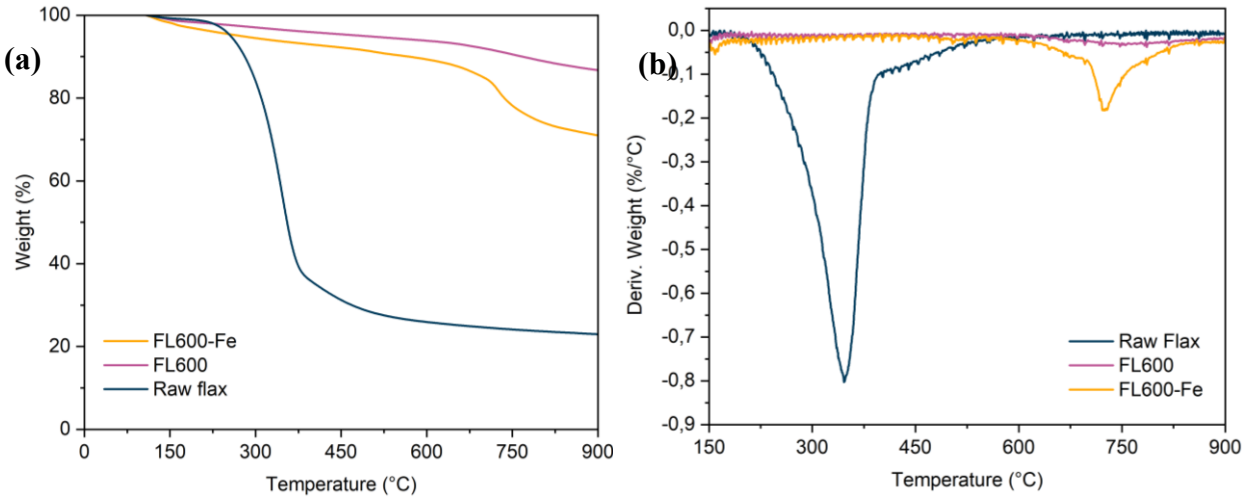

Figure 4.8: (a) TGA and (b) DTG curves of raw flax straw, pristine biochar (FL600), and FL600-Fe.

As depicted in Table 4.2, the moisture content of FL600-Fe exceeded that of both flax straw and pristine biochar. This observation can be attributed to the greater surface area and pore volume of the composite, as confirmed by the BET analysis results, facilitating an increased capacity for water adsorption (Álvarez et al., 2020). Following pyrolysis, volatile matter content decreased from 75.82% to 11.50% (FL600) and 25.68% (FL600-Fe), whereas the fixed carbon content significantly increased from 3.63% to 71.05% (FL600) and 47.06% (FL600-Fe). These findings confirm that a successful carbonization process took place through pyrolysis under the N_2 atmosphere. Nevertheless, the content of carbon decreased in the composite biochar due to challenges in carbon recovery caused by the high ash content (Álvarez et al., 2020; Nzediegwu, Naeth, et al., 2021). Usually, pyrolysis leads to a reduction in oxygen concentration, primarily due to the devolatilization process (Nzediegwu, Arshad, et al., 2021).

The pyrolysis of flax straw, resulting in both FL600 and FL600-Fe, led to enhanced carbonization, which was reflected by the reduction in the H/C, O/C, and (N+O)/C ratios. However, FL600-Fe exhibited higher atomic ratios in comparison to FL600, indicating an increase

in aromatic content, improved stability, and a higher presence of oxygen-containing functional groups (Uttran, 2018).

Table 4.2: Proximate analysis, elemental composition, and atomic ratios of raw flax straw, pristine biochar (FL600), and FL600-Fe.

Properties		**Raw Flax Straw**	**FL600**	**FL600-Fe**
TGA Analysis (%)	Moisture	1.21	1.76	3.34
	Volatile matter	75.82	11.50	25.68
	Ash	19.34	15.69	23.92
	Fixed Carbon	3.63	71.05	47.06
Elemental Composition (%)	C	44.97	80.15	51.62
	H	5.79	2.01	1.42
	N	0.71	0.98	0.81
	O	28.99	0.97	22.03
	S	<0.2	<0.2	<0.2
Atomic Ratio	H/C	1.55	0.30	0.33
	O/C	0.48	0.01	0.32
	(N+O)/C	0.50	0.02	0.33

4.1.9 Magnetic Properties

The magnetism of the pristine and Fe-loaded biochar detected using a SQUID magnetometer is presented in Figure 4.9. As expected, the pristine biochar showed no magnetic properties due to the lack of magnetic hysteresis loops. In contrast, the composite had a saturation magnetic field intensity of 7.40 emu g^{-1} at room temperature associated with the magnetic iron species content present on the catalyst as detected by XRD analysis. This finding potentially implies the possibility of easy separation from the solution using magnetic fields, resulting in great advantages for material recovery (Hsu et al., 2023; M. Sun et al., 2023). Similar studies involving

the synthesis of iron-biochar composites also reported a similar value of saturation magnetization (Guo et al., 2023; Pap et al., 2023).

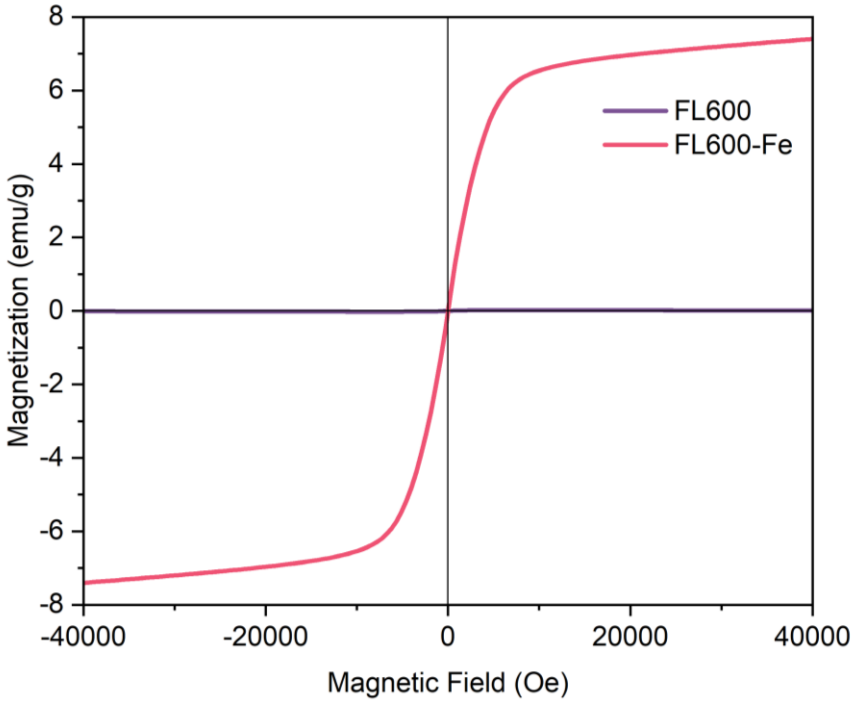

Figure 4.9: The magnetic hysteresis loops of pristine biochar (FL600) and FL600-Fe at 25 °C.

4.2 Adsorption Equilibrium

The FTIR spectra suggested the adsorption of some organic compounds on the surface of the composite after treatment (Figure 4.3). Consequently, before evaluating the FL600-Fe/PMS system on NAs degradation, the adsorption of fluorophore organic compounds at different time intervals using solely the composite was obtained by SFS analysis, as shown in Figure 4.10.

SFS was used for equilibrium experiments since real OSPW is a complex solution composed of high concentrations of contaminants such as naphthenic acids (NAs), suspended solids, inorganic salts, heavy metals, residual bitumen, and polycyclic aromatic hydrocarbons (Allen, 2008; Lévesque, 2014; Pourrezaei et al., 2014). Fluorescence intensity in SFS analysis can be observed in specific aliphatic compounds (including several NAs species), alicyclic carbonyls,

and highly conjugated double-bond compounds (Shu et al., 2014; C. Wang et al., 2016; Williams et al., 1983). Polycyclic aromatic hydrocarbons in OSPW display fluorescence and are composed of single, double, or multiple fused aromatic hydrocarbon rings (Shu et al., 2014). The hazardous nature of these contaminants is recognized to increase with greater molecular weight due to their ability to easily infiltrate cell membranes, posing a threat to living organisms (Ji et al., 2023; Mallah et al., 2022). Consequently, SFS analysis provides a semi-quantitative measurement of the concentration of organic fluorophore contaminants in OSPW and offers a reasonable indication of the effectiveness of a treatment.

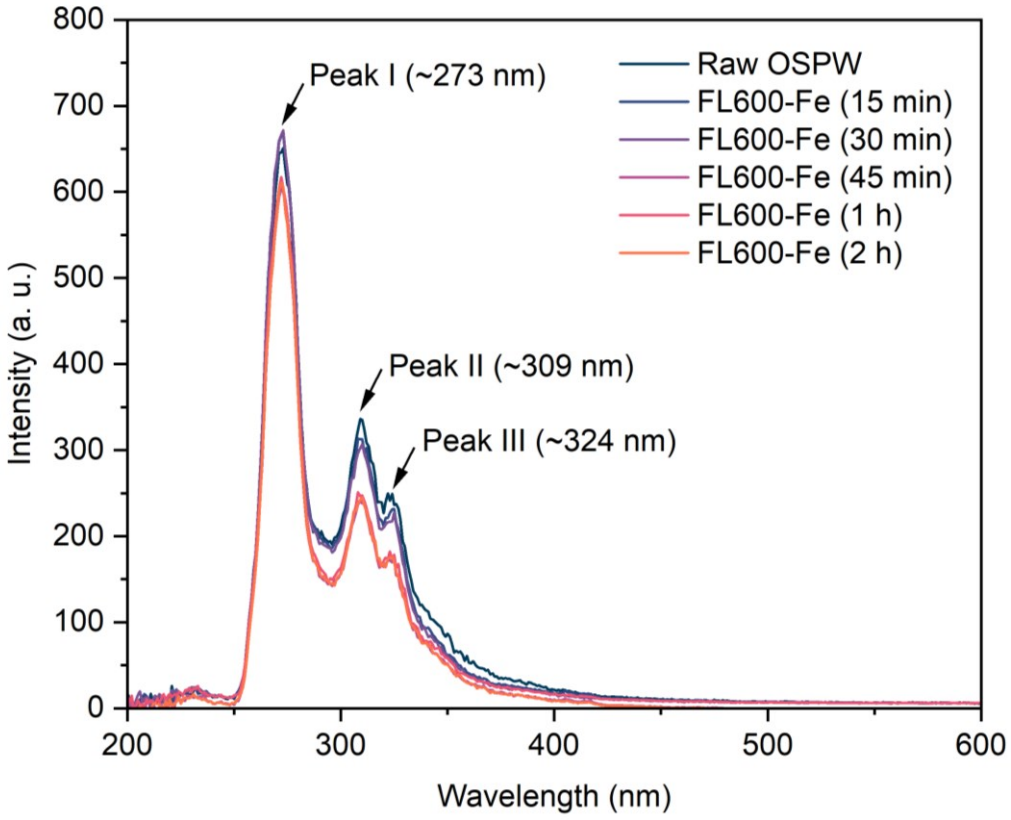

Figure 4.10: Adsorption of fluorophore organic compounds using FL600-Fe at different time intervals. FL600-Fe was used at a fixed dose of 1 g L^{-1}.

The SFS spectra profile of OSPW is characterized by 273, 309, and 324 nm peaks, representing simple-ring aromatic, two-ring aromatics, and three-ring aromatics, respectively. As observed, from 45 min, there is no significant further adsorption of fluorophore organic compounds. Therefore, this point of time was used to begin the catalytic PMS activation process for NAs removal in real OSPW. Additionally, these results prove that the composite alone is not efficient in removing these organic compounds from OSPW and needs PMS to initiate a synergetic effect for successful treatment, as confirmed by the control experiments performed for NAs removal.

4.3 Kinetic Experiments

4.3.1 Effect of Catalyst Dosage on Classical NAs Removal

Different ZV/biochar concentrations were evaluated to determine which would be the best dosage for the degradation of classical NAs. Four different concentrations of catalyst were used with a fixed concentration of 1 mM of PMS: 0.25, 0.5, 1, and 2 g L^{-1}. The results of the effect of FL600-Fe dose in classical NAs degradation are shown in Figure 4.11a. Using a biochar dose of 0.25 and 0.5 g L^{-1} (36.70% and 76.96% of classical NAs after 120 min, respectively) was not as outstanding as the removal achieved using the doses of 1 and 2 g L^{-1} (93.85% and 97.13% after 120 min, respectively). Even though the highest removal rate was achieved with a composite concentration of 2 g L^{-1}, employing half that concentration (1 g L^{-1}) still obtained a nearly equivalent degradation efficiency, beneficially reducing both production costs and material usage. Hence, the selection of 1 g L^{-1} as the best FL600-Fe dose was selected for the next experiments. The reaction followed a second-order kinetic as suggested by the R^2 values, as can be seen in Figure 4.11b.

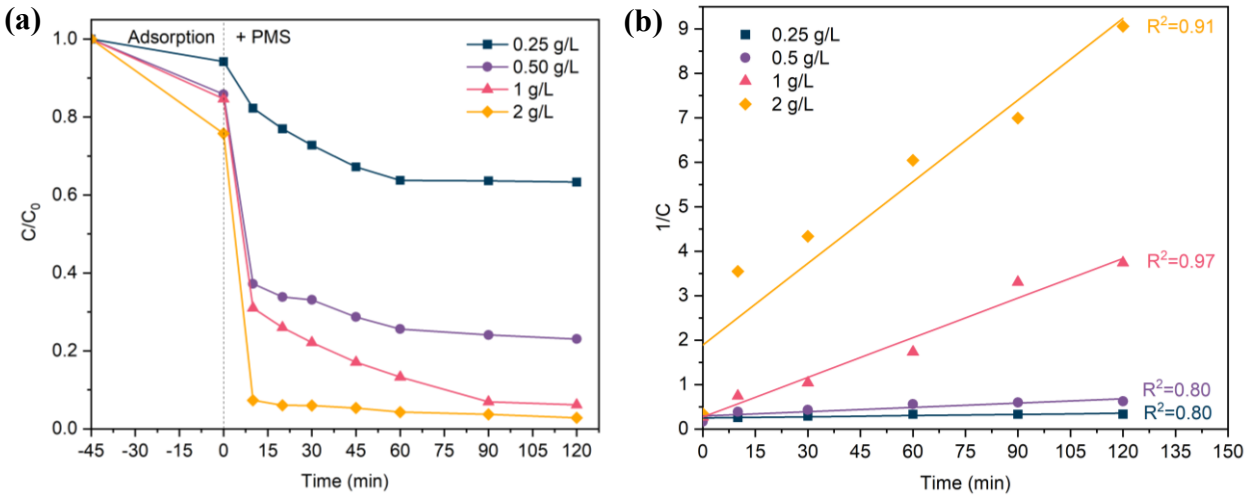

Figure 4.11: (a) Effect of FL600-Fe dosage on the degradation of classical NAs in real OSPW at a fixed concentration of PMS (1 mM) and (b) the corresponding second-order kinetic curve. Experimental conditions: [FL600-Fe] = 0.25, 0.5, 1, and 2 g L^{-1}; [PMS] = 1 mM; treatment time = 120 min.

4.3.2 Effect of PMS Dosage on Classical NAs Removal

Following the identification of the optimal catalyst dosage, the next step was to determine the optimal concentration of the oxidant for degrading classical NAs. Four different PMS concentrations (0.25, 0.5, 1, and 2 mM) were tested using a fixed FL600-Fe dose of 1 g L^{-1}. The results illustrating the impact of PMS dosage on the degradation of classical NAs can be seen in Figure 4.12. Using 0.25 and 0.5 mM of the oxidant for NAs degradation yielded removal rates of 43.60% and 57.28% after 120 min, respectively. However, these rates were not as remarkable as those achieved with 1 and 2 mM doses, which resulted in removal rates of 93.85% and 96.03% after 120 min, respectively. Similar to the effect of the catalyst dosage study, the highest removal rate was achieved with an oxidant concentration of 2 mM, but employing half that concentration (1 mM) still achieved nearly equivalent degradation efficiency. This approach not only reduces

production costs but also minimizes oxidant usage. The reaction followed a second-order kinetic as suggested by the R^2 values. Finally, the final selection of optimal doses of the system was 1 mM for PMS and 1 g L^{-1} for FL600-Fe.

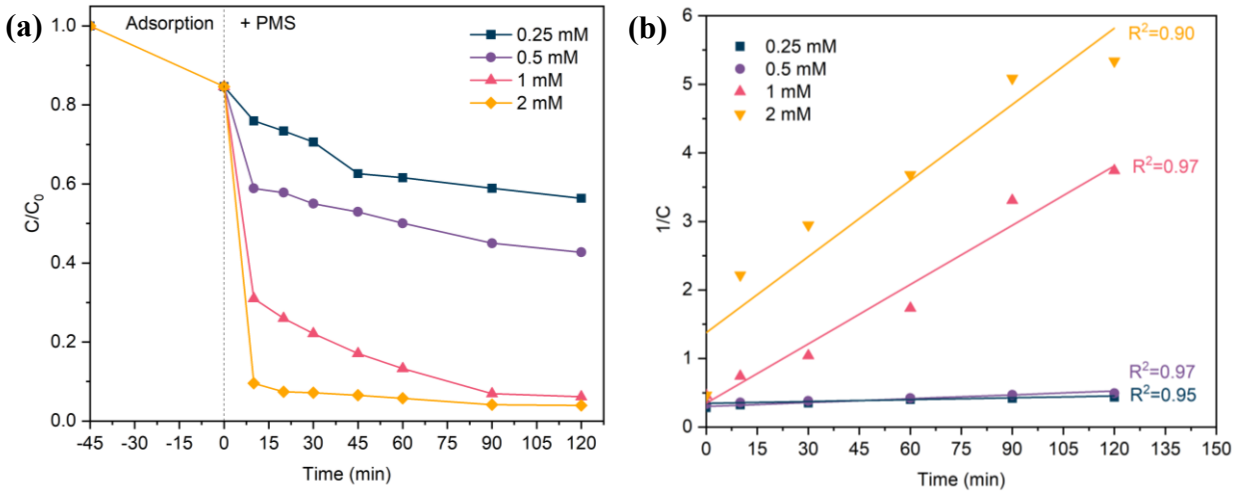

Figure 4.12: (a) Effect of PMS dosage on the degradation of classical NAs in real OSPW at a fixed concentration of the FL600-Fe (1 g L^{-1}) and (b) the corresponding second-order kinetic curve. Experimental conditions: [PMS] = 0.25, 0.5, 1, and 2 mM; [FL600-Fe] = 1 g L^{-1}; treatment time = 120 min.

4.3.3 Best Experimental Conditions and Control Experiments

As shown in Figure 4.13, the degradation of classical NAs using the optimal doses of the system (1 mM for PMS and 1 g L^{-1} for FL600-Fe) had an outstanding efficiency of 93.9% after 120 min of treatment. The adsorption of classical NAs with pristine biochar demonstrates a low efficiency of 19.77% even after 165 minutes. Similarly, FL600-Fe achieves a low efficiency of 15.57% after 45 min and equilibrates at 24.12% after 165 min in the absence of PMS in the matrix, while the NAs removal using only PMS achieves an efficiency of 27.17% after 120 min. As observed in Figure 4.13a, there is a significant reduction when PMS is introduced to the OSPW solution with the composite, confirming a synergetic effect from the FL600-Fe/PMS system.

Studies evaluating the use of ZVI composite to activate PMS for organic contaminant degradation constantly reported high efficiencies, often approaching 100%, along with the presence of synergistic effects (H. Sun et al., 2023; Y. Zhang et al., 2021). Although many of these reports indicate the attainment of removal equilibrium within 1 hour with less dosage, it is important to note that the present study uses a real matrix with a complex chemical composition and a wide variety of organic contaminants (C. Li et al., 2017). This complexity makes the degradation process more challenging than simplified model compound matrices.

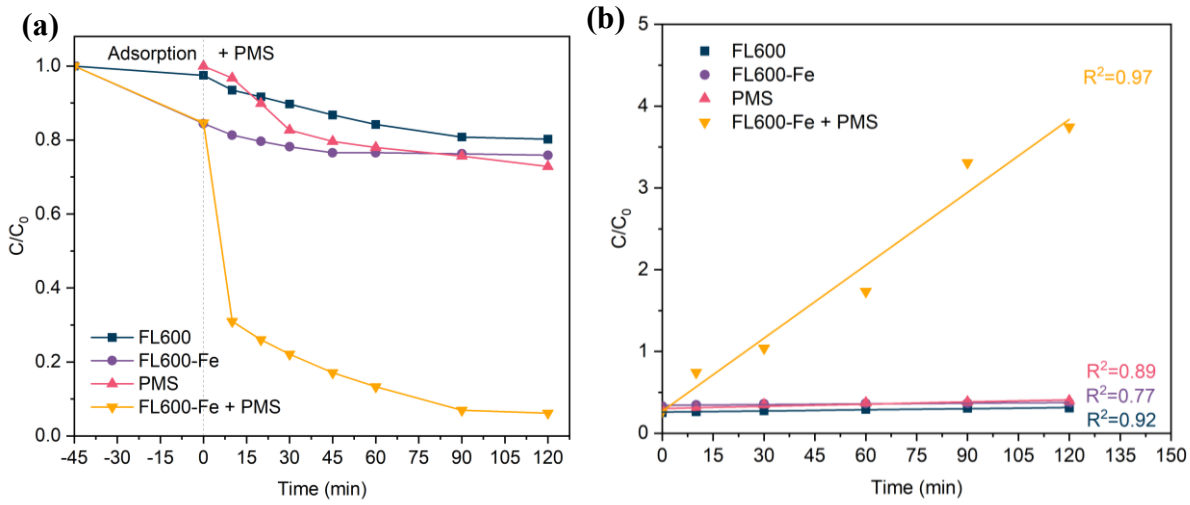

Figure 4.13: (a) Control experiments for comparison with the synergistic effect obtained by the FL600-Fe/PMS system in terms of classical NAs removal from real OSPW and (b) the corresponding second-order kinetic curve. Experimental conditions: [PMS] = 1 mM; [FL600] = [FL600-Fe] = 1 g L^{-1}; treatment time = 120 min.

The efficiency of the FL600-Fe/PMS system was also evaluated for the degradation of fluorophore organic compounds in real OSPW using SFS analysis (Figure 4.14). After 90 min, the peak for first-ring aromatics was greatly reduced while the peaks corresponding to two and three-

ring aromatics almost completely disappeared. These results are very consistent with the previous analysis of the degradation of classical NAs in OSPW.

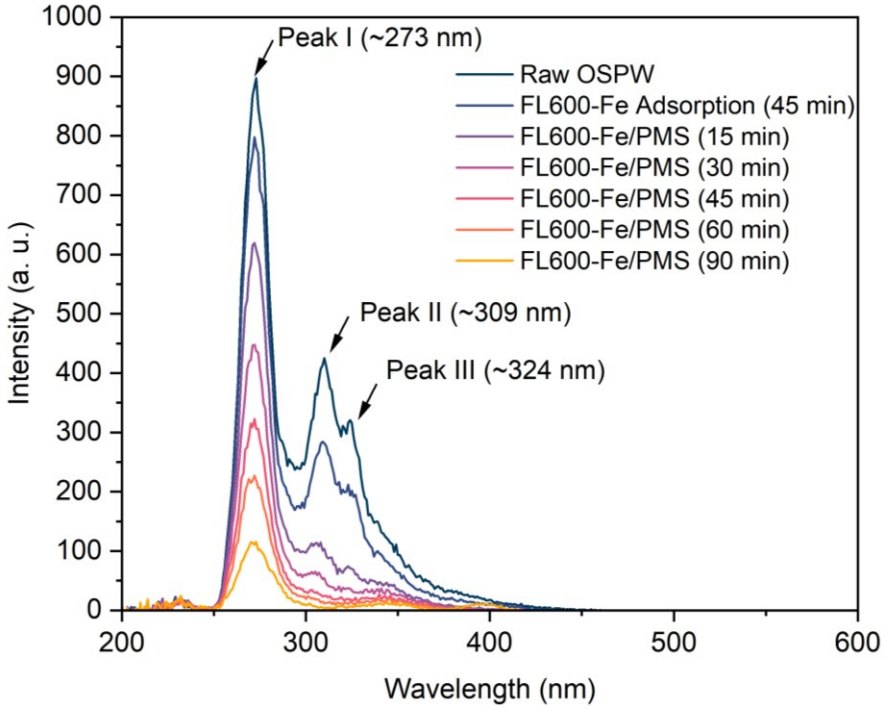

Figure 4.14: Degradation of fluorophore organic compounds using the FL600-Fe/PMS system at optimal doses for different time intervals using SFS analysis. Experimental conditions: [PMS] = 1 mM; [FL600-Fe] = 1 g L^{-1}.

The next step involved assessing the effectiveness of the FL600-Fe/PMS system for total NAs removal in real OSPW. The NAs in the OSPW were categorized according to their oxygen number (O_x-NAs), where x = 2 represented classical NAs, and values of 3 to 6 corresponded to oxidized NAs (R. Huang et al., 2015; Meshref et al., 2017). The raw OSPW used in this study had a total NAs concentration of 15.76 mg L^{-1} (Table 4.1), and the results of NAs removal from raw OSPW are presented in Figure 4.15. The highest removal efficiency for NAs was notably observed in the case of classical NAs, which also constitute the predominant fraction of NAs in the untreated OSPW (Table 4.1). The efficiency of NAs decreased with increasing oxygen number, likely

associated with the radicals generated by the FL600-Fe/PMS system. As suggested by EPR and quenching results (discussed in the next section), the •OH species play a crucial role in degradation and might generate by-products with added oxygen atoms (hydroxylated by-products) compared to the original compound, in contrast to systems where $SO_4^{\bullet-}$ species are more prevalent (Fang et al., 2019; Tang, 2003). Therefore, these results might suggest that the •OH radical generated formed O_{X+1}-NAs species (where $2 \leq x \leq 6$). Furthermore, some studies have even reported an increase in the concentration of oxidized NAs after OSPW treatment (Fang et al., 2018, 2019; Y. Zhang et al., 2016).

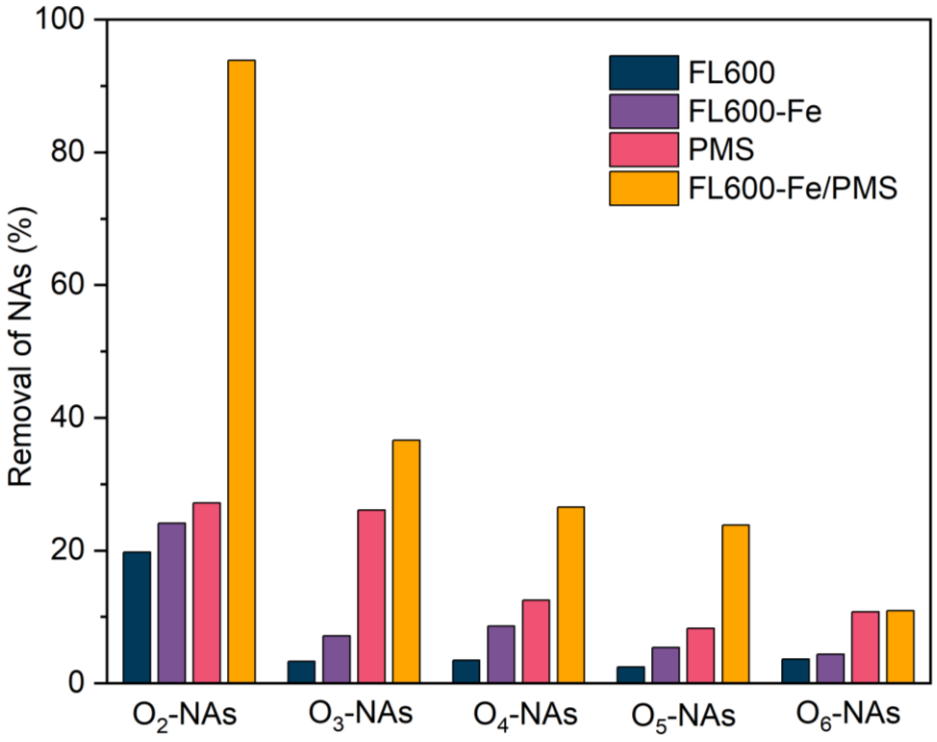

Figure 4.15: Removal efficiency of classical NAs (O_2-NAs) and oxidized NAs (O_3-, O_4- O_5- and O_6-NAs) using the pristine biochar (FL600), FL600-Fe, the oxidant (PMS), and the FL600-Fe/PMS system. Experimental conditions: [PMS] = 1 mM; [FL600] = [FL600-Fe] = 1 g L^{-1}; treatment time = 120 min.

(a)

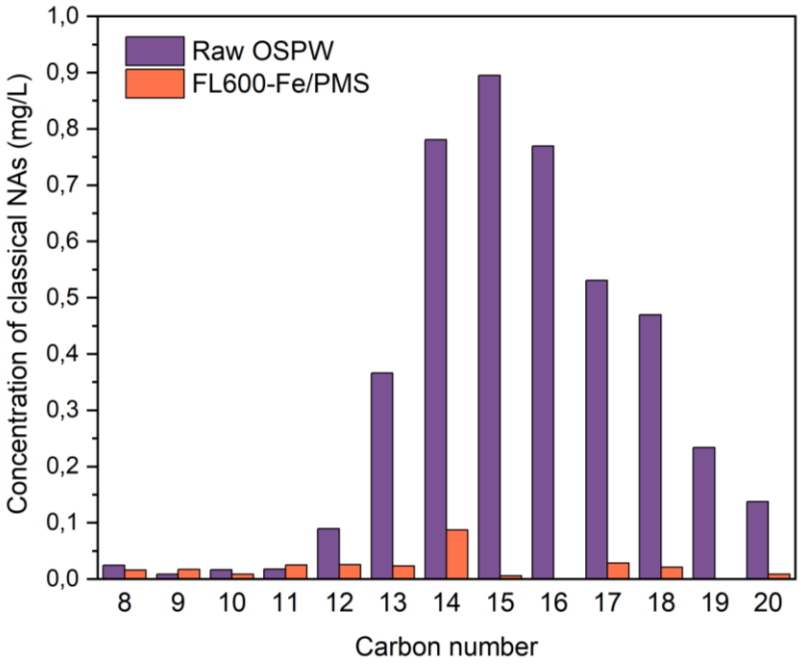

(b)

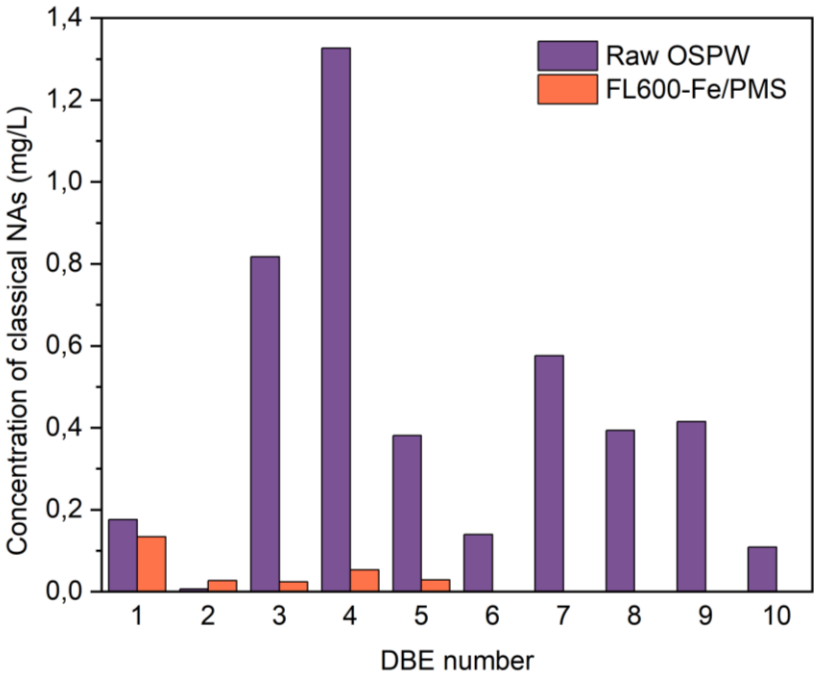

Figure 4.16: Concentration of classical NAs in terms of (a) carbon number and (b) DBE number in raw OSPW and treated biochar using the FL600-Fe/PMS system. Experimental conditions: [PMS] = 1 mM; [FL600] = [FL600-Fe] = 1 g L^{-1}; treatment time = 120 min.

Finally, the concentration profile of classical NAs as a function of carbon and DBE number in raw and treated OSPW is shown in Figure 4.16a and 4.16b, respectively. The classical NAs ($C_nH_{2n+Z}O_2$) were classified based on their carbon number ($7 \leq n \leq 26$) and their double bond equivalency (DBE) number (where DBE = 1 – Z/2, in which Z is the hydrogen deficiency number resulting from ring or double bond formation, $0 \leq -Z \leq 24$) (Cancelli & Gobas, 2022; R. Huang et al., 2015; Meshref et al., 2017). The range of carbon numbers 13 to 18 represented 87.8% of all classical NAs in raw OSPW, in which carbon number 15 represented 20.6% of classical NAs. The highest concentration in terms of DBE number was given by DBEs 3, 4, and 7, representing 18.9, 30.6, and 13.3% of classical NAs, respectively. Therefore, most classical NAs in this raw OSPW were bicyclic, tricyclic, and heptacyclic (Benally et al., 2019). The concentration of these compounds in OSPW was greatly reduced, meaning that the FL600-Fe/PMS system is a promising treatment to assist in the degradation of NAs from real OSPW.

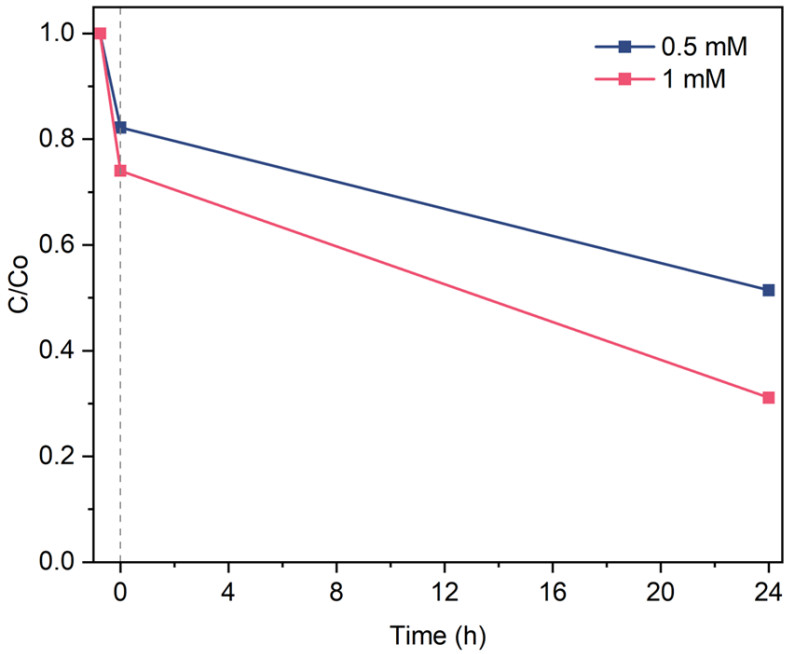

Figure 4.17: Degradation of classical NAs using 0.1 g L^{-1} of FL600-Fe, plus 0.5 mM and 1 mM of PMS for 24 h.

Additionally, Figure 4.17 shows experiments using a smaller concentration of the composite (0.1 g L^{-1}) at two PMS doses (0.5 and 1 mM) for 24 h. Results indicate that fairly good results are obtained when the system doses are decreased and treatment time increases. Specifically, using 0.5 mM and 1 mM of PMS achieved 49.0% and 68.0% degradation of classical NAs, respectively. These findings suggest a better approach for scale-up applications in which less material reduces production costs.

Unlike other studies in the literature, the current work focuses on activating PMS solely through the ZVI particles present on the biochar surface, without relying on any distinct external activation sources, such as artificial UV light or pre-existing components within the feedstock. For example, Sánchez-Montes et al. (2024) investigated the activation of PMS using UVA LED light for real OSPW treatment, achieving an 80% degradation efficiency of classical NAs after 60 min. Despite this, it is well known that use of artificial light sources increases the overall cost of the process. Song et al. (2022) conducted experiments employing a sludge biochar modified with iron oxide to activate PMS to remove model NAs compounds. The outcome proved to be highly promising, mainly attributed to the existing presence of transition metals in the sludge. This composition helps to enhance the oxidant activation, thus achieving better degradation efficiencies. Nevertheless, the utilization of these feedstocks for biochar production is frequently linked to secondary contamination arising from the presence of these pre-existing elements. Consequently, the feedstock plays an important role in a biochar/PMS system due to inherent components that can offer substantial benefits or even disadvantages to the process.

4.4 Oxidant Consumption

The oxidant consumption at determined time intervals was quantified to determine the residual concentration of the oxidant in the solution. As shown in Figure 4.18, the initial PMS

concentration of 1 mM decreased to 0.47 mM after 120 min, indicating that 53.0% of the PMS remained within the matrix due to incomplete reaction. This concentration of residual oxidant is expected to be consumed shortly afterward and did not significantly affect the microbial viability assay performed for the FL600-Fe/PMS system. Specifically, in the context of pools, spas, and hot tubs, residual PMS is beneficial and used as an alternative to chlorine to maintain or restore water clarity by oxidizing organic contaminants and impurities in water (Anipsitakis et al., 2008). Therefore, it is expected that any remaining PMS concentration within the matrix will be quickly consumed or activated by light (UV or solar natural radiation) or heat (Arslan et al., 2023; Fang et al., 2019; Saha et al., 2023) and will lead to further degradation of remaining organic contaminants in OSPW.

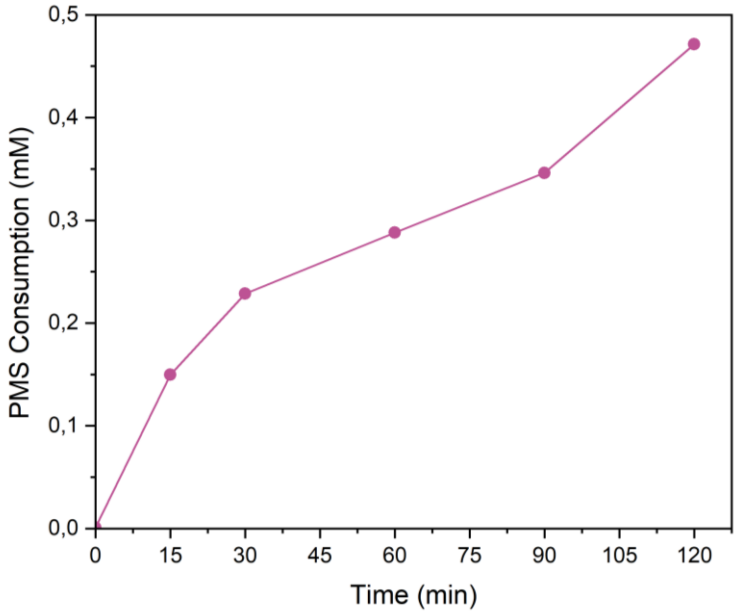

Figure 4.18: PMS Consumption at time intervals using the FL600-Fe/PMS system. Experimental conditions: [PMS] = 1 mM; [FL600-Fe] = 1 g L^{-1}; treatment time = 120 min.

4.5 Role of Reactive Radicals in the FL600-Fe/PMS System

4.5.1 Quenching Experiments

Quenching experiments were performed to evaluate the effect of radical species generated during the activation of PMS using FL600-Fe on the degradation of NAs from real OSPW. Briefly, 0.4 M of isopropanol (IPA) was used to scavenge both $^{\bullet}OH$ and $SO_4^{\bullet-}$ species by a second-rate constant of $k = 2.8\times10^9$ M^{-1} s^{-1} and $k = 6.0\times10^7$ M^{-1} s^{-1}, respectively. Additionally, 0.4 M *t*-butyl alcohol (TBA) was also used to scavenge $^{\bullet}OH$ species using a second-rate constant of k = 3.8-7.6×10^8 M^{-1} s^{-1} (Liang & Su, 2009). Figure 4.19 illustrates that the removal efficiency of classical NAs using the FL600-Fe/PMS system decreased when using both scavengers, implying that the degradation mechanism in this system relies significantly on both species. Under the selected conditions, the system achieves a 93.85% degradation efficiency. Nevertheless, when IPA and TBA were introduced, the efficiency markedly decreased to 19.2% and 33.5%, respectively. This leads to the conclusion that in this study, $^{\bullet}OH$ species exhibited greater prominence compared to $SO_4^{\bullet-}$ species, as corroborated by EPR analysis. Moreover, at neutral and basic pH matrices, the abundance of $OH^{\bullet}$ species can provoke a reaction with $SO_4^{\bullet-}$ as described by equation 4.1 (Dong et al., 2019; Liang & Su, 2009; Song et al., 2022):

$$SO_4^{\bullet-} + OH^- \rightarrow SO_4^{2-} + {}^{\bullet}OH \qquad (4.1)$$

Similar results were also observed by Song et al. (2022) and Xu et al. (2020), where $OH^{\bullet}$ played a dominant role in the removal of organic contaminants using a Fe-loaded biochar and PMS system for the elimination of organic contaminants. As discussed in subsection 4.3.3, the formation of hydroxylated by-products by $^{\bullet}OH$ species during the degradation of classical NAs from OSPW results in an elevated concentration of oxidized NAs, consequently reducing the removal efficiency of these compounds (Fang et al., 2019; Tang, 2003).

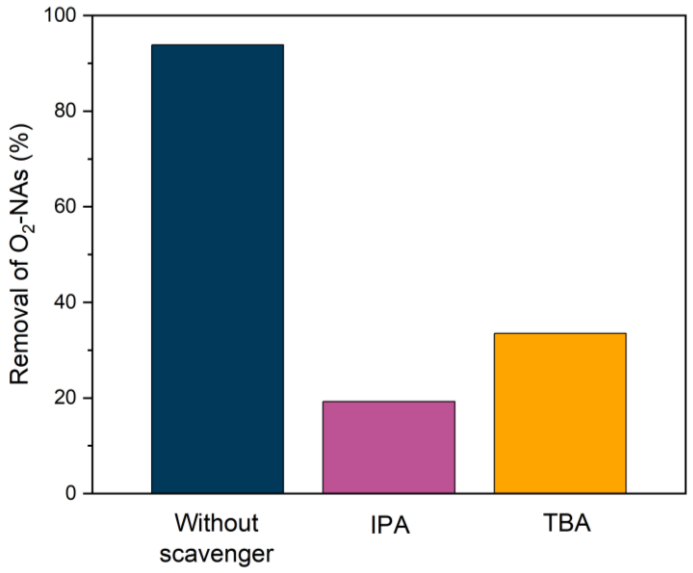

Figure 4.19: Removal of classical NAs using the FL600-Fe/PMS system in the absence and presence of IPA and TBA. General conditions: [IPA] = 0.4 M; [TBA] = 0.4 M; [PMS] = 1 mM; [FL600-Fe] = 1 g L^{-1}; treatment time = 120 min.

4.5.2 Identification of Radicals by EPR Spectroscopy

EPR analysis was conducted to identify the reactive oxygen species (ROS) generated during the PMS activation using FL600-Fe, which played a key role in the degradation of NAs in OSPW. DMPO and BMPO were used as trapping agents to confirm the role of $^{\bullet}OH$, $SO_4^{\bullet-}$, and $O_2^{\bullet-}$ in the system. Similar studies found the three contemplated radicals through EPR analysis while using transition metals supported on biochar to activate PMS for the degradation of organic contaminants in industry wastewater (Z. Huang et al., 2019; F. Meng et al., 2023). Figure 4.20a shows two different groups of peaks, with the first group showing four equidistant intense peaks with an approximate ratio of 1:2:2:1 (● peaks), characteristic of the DMPO$^{\bullet}$-OH spectra, and the second group displaying six even peaks with less intensity (▼ peaks), corresponding to DMPO$^{\bullet}$-OSO_3H. Similarly, Figure 4.20b displays two groups of peaks, with both sets showing four equidistant peaks for BMPO$^{\bullet}$-OH (○ peaks) and BMPO-$O_2^{\bullet-}$ (◆ peaks). Therefore, the spectra

have all three contemplated ROS species that were involved in the degradation of NAs in real OSPW using the FL600-Fe/PMS system. These results correlate with the radicals identified in the quenching experiments performed in this study.

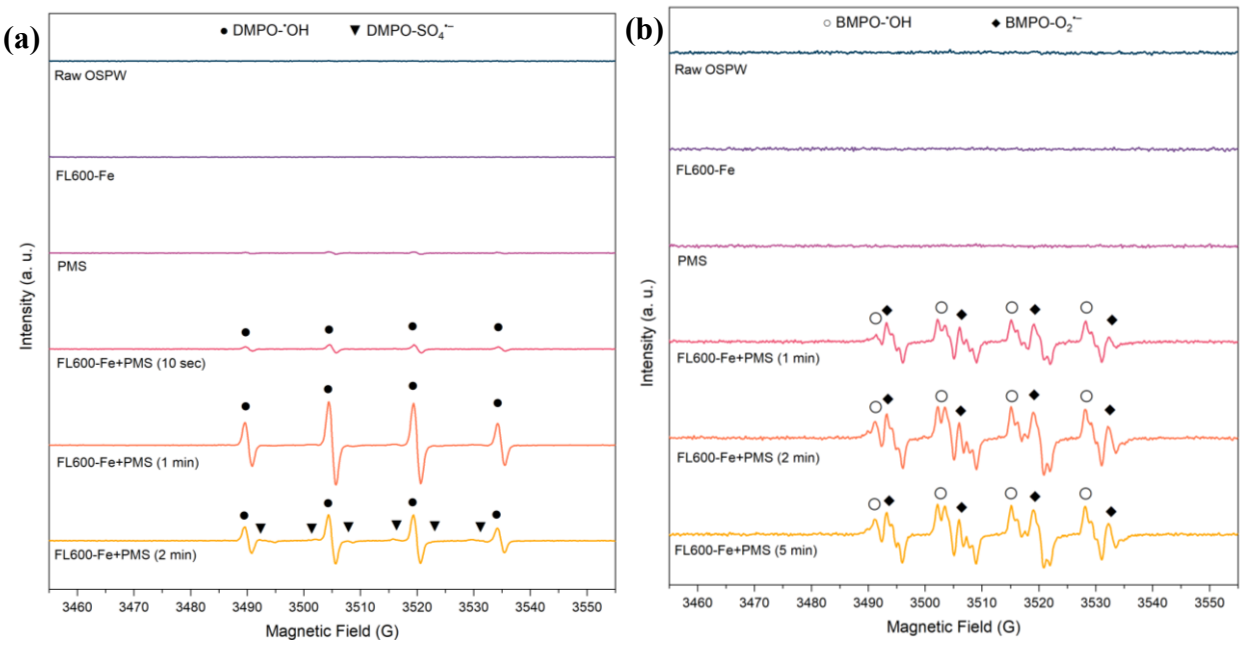

Figure 4.20: EPR Spectra of the FL600-Fe/PMS system in real OSPW using (a) DMPO for •OH and $SO_4^{\bullet-}$ identification, and (b) BMPO for •OH and $O_2^{\bullet-}$ identification. Experimental conditions: [PMS] = 1 mM; [FL600-Fe] = 1 g L^{-1}; [DMPO] = 50 mM; [BMPO] = 50 mM.

4.6 Leaching of Metals from Composite to OSPW During Treatment

Metal-based catalysts are widely applied in catalytic processes due to their low leaching tendency, which prevents secondary pollution caused by the uncontrolled release of metals into the environment (Kohantorabi et al., 2021; C. Zhao et al., 2021). In degradation processes, leaching ions into the matrix is insufficient to activate PMS and may compromise the efficiency of the system (S. Xiao et al., 2020). Furthermore, regulations and standards aimed at protecting water resources and aquatic ecosystems limit the concentration of certain metals in treated water (Canadian Council of Ministers of the Environment, 1987). Therefore, it was indispensable to

assess the long-term stability and efficiency of the synthesized catalyst through leaching tests to confirm the properties of the composite.

Kohantorabi et al. (2021) concluded that carbon-based materials show high efficiency and low leaching issues compared to other carriers, as well as suggesting that the physicochemical characteristics and the production method of the catalyst play a crucial role in metal release during the degradation. In this study, the initial concentration of iron in raw OSPW was observed to be below the limit of detection and quantification of the technique, which are 0.001 and 0.005 mg L^{-1}, respectively. Similarly, the concentration of leached iron present in the treated samples with FL600-Fe at 45 min and the FL600-Fe/PMS system at 120 min were also both below the limit of detection and quantification. Based on the results, the effective removal of NAs by the PMS activation with Fe-loaded biochar is attributable to the iron ions present on the solid surface of the biochar nanocarrier rather than iron present in the solution due to leaching. Additionally, iron leaching into the solution during treatment is significantly below the minimum concentration of iron (0.3 mg L^{-1}) established by the guidelines of the Canadian Council of Ministers of the Environment for freshwater (Canadian Council of Ministers of the Environment, 1987). Similarly, studies performed by Shi et al., (2023) and Xu et al. (2024) concluded that biochar as a nanocarrier for metal PMS activation inhibits ion release and improves the stability of the composite in the degradation of micropollutants from water. In this context, the produced composite in the present study is a catalyst that has excellent chemical stability caused by the strong interaction between iron ions and the nanocarrier material.

Further experiments were conducted to evaluate iron leaching in OSPW treatment over a 24-hour period using the optimal doses determined previously. The findings revealed that after this duration, the concentration of iron ions measured at 0.041 mg L^{-1}, consistently remaining

below the recommended guidelines for freshwater (Canadian Council of Ministers of the Environment, 1987).

4.7 Microbial Viability Assay

The toxicity before and after treatment was evaluated through a 21-hour microbial viability assay of the *Staphylococcus warneri* bacteria. This assessment significantly differs from other studies that evaluate the efficiency of treatments in reducing OSPW toxicity through the use of Microtox® bioassay (C. Li et al., 2017; Medeiros et al., 2023; Suara et al., 2022). Microtox® is a commonly used technique that assesses toxicity following exposure for only 5 and 15 min, primarily detecting acute toxicity and immediate effects rather than the longer-term impacts of toxic substances, including genotoxic effects, which may affect cell viability over extended periods (Zani et al., 2005). Furthermore, this bioassay evaluates the decline in cell density through luminescence detection. However, when dealing with complex mixtures such as OSPW, it is common to observe luminescence reductions that do not necessarily correlate with a substantial effect on cell growth (Gellert, 2000). On the other hand, the 21-hour microbial viability assay used in this study covers a significantly longer period, allowing for the detection of cumulative effects in growth after exposure.

The positive control shown in the results of Figure 4.21 contains compounds that inhibit the growth of the culture and is considered as 0% viability. After 21 h of exposure to the untreated sample, the reduction observed was nearly 3.5 Log (10,000-fold) below the control ($P<0.01$), indicating that the raw OSPW contains components that are toxic to bacteria and partially inhibit their growth. On the other hand, the treated OSPW exhibited an average Log Reduction of 0.28, showing a difference of 1.3 Log (82.09%) and 4.8 Log (94.36%) when compared to the untreated sample and the positive control, respectively. The results suggest that the treatment shows no

significant reduction in bacterial growth, and therefore, the presence of residual organic components in OSPW after treatment does not have a marked effect on bacterial viability during the observed incubation period.

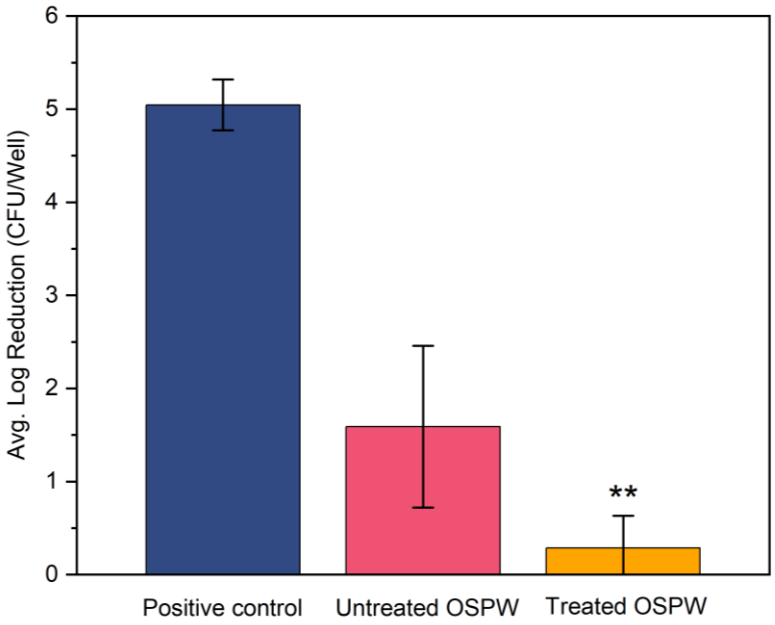

Figure 4.21: Average Log growth of *Staphylococcus warneri* following a 21-hour exposure to untreated and treated OSPW. The significance level of $P<0.01$ was represented by (**). Experimental conditions: [PMS] = 1 mM; [FL600-Fe] = 1 g L^{-1}; treatment time = 120 min.

4.8 Removal of Bioavailable Acid Extractable Organics (AEOs)

The BE-SPME technique was performed to assess the bioavailability of AEOs, which include hydrocarbons and other organisms such as NAs. Previously, Whale et al., 2022 quantified the toxicity of oil refinery wastewater by bioassays and BE-SPME and suggested that both tests have the potential to assist as screening tools for toxicity assessment. Additionally, Huang et al. (2021) proposed the BE-SPME method as a valuable alternative to characterize the bioavailability of AEOs for toxicity prediction in OSPW.

As shown in Figure 4.22, there was approximately a 75.0% reduction in the bioavailability of AEOs in OSPW after FL600-Fe/PMS treatment at optimal conditions. This reduction is potentially linked to the increase in the viability of the *Staphylococcus warneri* bacteria after FL600-Fe/PMS treatment. Similarly, Medeiros et al., 2023 found that the acute toxicity quantified using Microtox® bioassay and bioavailable AEOs in real OSPW had a 66.0% and 91.0% reduction, respectively, after adsorption treatment using Zinc-modified biochar. Therefore, the integration of both bioassays and BE-SPME analysis offers a promising approach to measure the residual toxicity in OSPW due to remaining organic compounds.

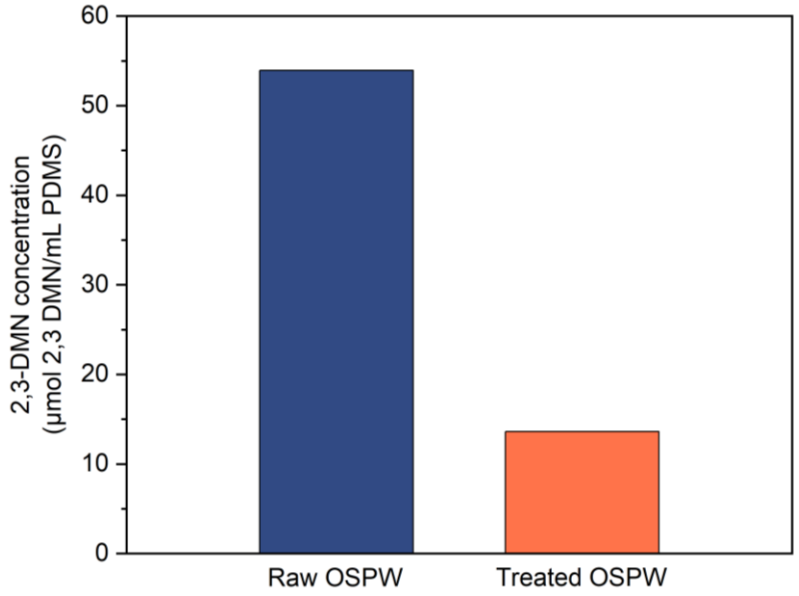

Figure 4.22: Concentration of bioavailable acid extractable organics in raw and untreated OSPW measured by BE-SPME. Experimental conditions: [PMS] = 1 mM; [FL600-Fe] = 1 g L^{-1}; treatment time = 120 min.

4.9 Regeneration and Reuse of Spent Composite

The regeneration of spent FL600-Fe had two main purposes: to break the bonds between the adsorbed NAs in the surface of the composite and to reload ZVI particles. Specifically, the

pollutant molecules are volatilized through thermal regeneration to reduce the risk of secondary pollution. Additionally, the regeneration and reuse of the composite helps to reduce the costs associated with the production of new particle carrier. Four cycles of thermo-regeneration at 600°C were performed for the composite, and the results are presented in Figure 4.23. The degradation efficiency with fresh material achieved a 93.9% degradation of classical NAs from raw OSPW using the best conditions. After the first cycle of regeneration, the degradation efficiency decreased to 75.0% and kept decreasing to 52.2% in the fourth cycle. Previous studies suggest that this decrease in the degradation capacity after thermal regeneration is due to the modification of the chemical and pore structure of the biochar. As described in Section 4.3.3, the pristine biochar achieved a 19.8% degradation efficiency, confirming the potential of regenerated FL600-Fe by its superior efficiency compared to the unmodified material.

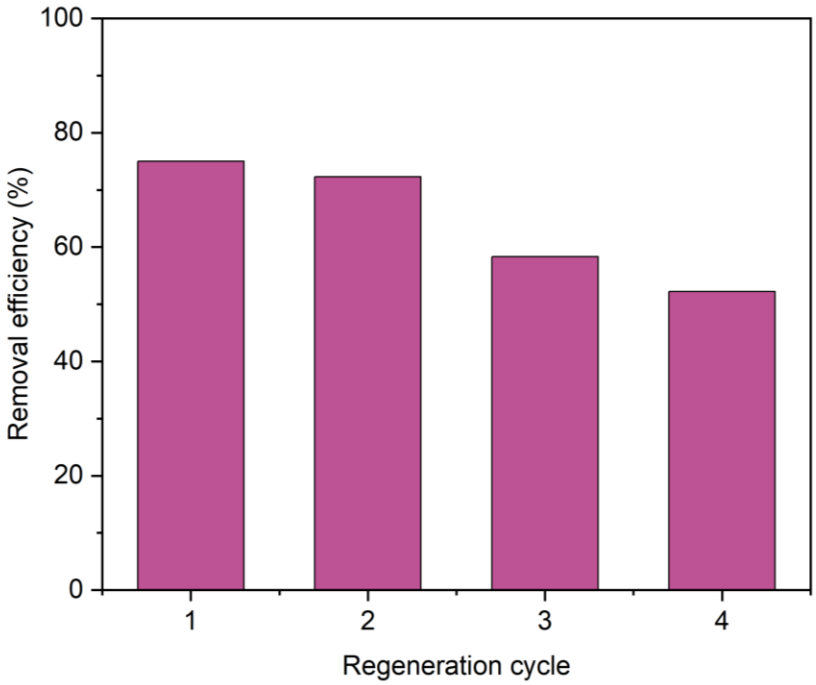

Figure 4.23: Degradation efficiency of regenerated and reused FL600-Fe for the removal of classical NAs from real OSPW. Experimental conditions: [PMS] = 1 mM; [FL600-Fe] = 1 g L^{-1}; treatment time = 120 min.

CHAPTER 5 Conclusions

The results obtained in this thesis show the capability of the ZVI composite derived from flax straw to activate PMS to efficiently degrade NAs from real OSPW. The literature review highlights the ongoing research on related technologies.

The first focus of this study was to conduct an in-depth characterization of the ZVI/biochar composite. Thus, raw flax straw, pristine biochar, and the composite biochar were characterized using BET, zeta potential, FESEM, FTIR, XRD, XPS, TGA, ultimate analysis, and SQUID magnetization. The carbonization and the presence of ZVI particles in the modified biochar were validated by FTIR, FESEM, XRD, and XPS analyses. BET, TGA, and ultimate analysis provided valuable information about the physical properties and content of the samples, such as the elemental composition, surface area, and thermostability. The zeta potential values helped to assess the stability of the composite and its potential to be applied without the formation of agglomerates, as well as its high electrostatic interaction with the PMS. SQUID magnetization curve assisted in understanding the magnetic properties of the composite, which could improve its recovery from the treated matrix by an external magnetic field in future applications.

As a second objective, SFS analysis was conducted to determine the adsorption equilibrium time of the composite in OSPW PMS. In terms of classical NAs removal, the best dosages of the composite and PMS were found to be 1 g L^{-1} and 1 mM, respectively. The second-order kinetic model best fits the degradation of classical NAs, resulting in a remarkable efficiency of 93.9% after 120 min of treatment using the best doses for the composite and oxidant. The synergetic effect in the treatment was observed after comparing the degradation results of the coupled system and the control experiments, i.e., the individual processes. The high degradation of the FL600-Fe/PMS system was attributed to the generation of $^{\bullet}OH$, $SO_4^{\bullet-}$, and $O_2^{\bullet-}$ species, which were identified

using radical scavengers and EPR measurements. Furthermore, secondary contamination associated with the iron leached from the material into the solution was quantified below the limit of detection of the instrument and significantly below the concentration recommended by the Canadian Council of Ministers of the Environment for freshwater. Moreover, a microbial viability assay based on longer exposure period compared to conventional bioassays was performed to evaluate the environmental compatibility of the treated OSPW by the proposed treatment in this study. Results indicated an 82% increase in *Staphylococcus warneri* bacteria growth, indicating that the pre-existing toxic effect of OSPW was greatly reduced after treatment. Additionally, the treatment resulted in a 75% reduction in the concentration of bioavailable AEOs (such as NAs, and neutral and ionizable hydrocarbons), which are organic compounds that contribute to the toxicity of OSPW. One drawback of this system is the necessity for regeneration before reuse, as the ZVI particles are depleted during the treatment process. Regeneration results show potential for reuse purposes, reducing costs associated with production in scale-up processes; however, the stability of the spent material needs to be further improved. Finally, the findings of this study confirm that the PMS activation using the FL600-Fe composite holds promise as an efficient, cost-effective, and environmentally friendly method for removing NAs for OSPW reclamation.

CHAPTER 6 Recommendations and Future Perspectives

Future perspectives in OSPW treatment must include complete approaches to address the environmental challenges associated with remediation. In this sense, research and innovation must focus on advancing sustainable and cost-effective treatment methods for OSPW, with an emphasis on reducing the ecological impact, promoting resource recovery, and ensuring regulatory compliance. This study provides the foundational basis for future research exploring the degradation of NAs in OSPW by utilizing ZVI-loaded biochar derived from agricultural waste to activate PMS. Additional experiments aimed to lower the concentration of the catalyst and the oxidant could be performed at longer contact times for further optimization of production costs. A useful area of investigation would involve a more in-depth assessment of the removal rates of BC-Fe at varying preparation temperatures, as this parameter is crucial due to the substantial influence of feedstock type and synthesis operation conditions on the ZVI production and PMS activation. Furthermore, the utilization of magnetic properties could serve for the separation of the composite from the solution and facilitate experiments related to regeneration and reusability.

Finally, the integration of cutting-edge technologies, efficient and scalable treatment processes, and the development of robust monitoring systems will be key in the search for environmentally responsible solutions. OSPW treatment using biochar composites holds the promise of developing highly efficient and sustainable solutions. Therefore, bench and pilot-scale experiments should be performed to open the way towards the scaling-up applications of these materials in wetlands to contribute to OSPW reclamation efforts.

Bibliography

Abdalrhman, A. S., & Gamal El-Din, M. (2020). Degradation of organics in real oil sands process water by electro-oxidation using graphite and dimensionally stable anodes. *Chemical Engineering Journal*, *389*, 124406. https://doi.org/10.1016/j.cej.2020.124406

Allen, E. W. (2008). Process water treatment in Canada's oil sands industry: I. Target pollutants and treatment objectives. *Journal of Environmental Engineering and Science*, *7*(2), 123–138. https://doi.org/10.1139/S07-038

Álvarez, M. L., Gascó, G., Palacios, T., Paz-Ferreiro, J., & Méndez, A. (2020). Fe oxides-biochar composites produced by hydrothermal carbonization and pyrolysis of biomass waste. *Journal of Analytical and Applied Pyrolysis*, *151*, 104893. https://doi.org/10.1016/j.jaap.2020.104893

Anipsitakis, G. P., & Dionysiou, D. D. (2003). Degradation of Organic Contaminants in Water with Sulfate Radicals Generated by the Conjunction of Peroxymonosulfate with Cobalt. *Environmental Science & Technology*, *37*(20), 4790–4797. https://doi.org/10.1021/es0263792

Anipsitakis, G. P., Tufano, T. P., & Dionysiou, D. D. (2008). Chemical and microbial decontamination of pool water using activated potassium peroxymonosulfate. *Water Research*, *42*(12), 2899–2910. https://doi.org/10.1016/j.watres.2008.03.002

Arslan, M., & Gamal El-Din, M. (2021). Bacterial diversity in petroleum coke based biofilters treating oil sands process water. *Science of The Total Environment*, *782*, 146742. https://doi.org/10.1016/j.scitotenv.2021.146742

Arslan, M., Ganiyu, S. O., Lillico, D. M. E., Stafford, J. L., & Gamal El-Din, M. (2023). Fate of dissolved organics and generated sulfate ions during biofiltration of oil sands process

water pretreated with sulfate radical advanced oxidation process. *Chemical Engineering Journal*, *458*, 141390. https://doi.org/10.1016/j.cej.2023.141390

Arslan, M., Müller, J. A., & Gamal El-Din, M. (2022). Aerobic naphthenic acid-degrading bacteria in petroleum-coke improve oil sands process water remediation in biofilters: DNA-stable isotope probing reveals methylotrophy in Schmutzdecke. *Science of The Total Environment*, *815*, 151961. https://doi.org/10.1016/j.scitotenv.2021.151961

Ayoub, K., van Hullebusch, E. D., Cassir, M., & Bermond, A. (2010). Application of advanced oxidation processes for TNT removal: A review. *Journal of Hazardous Materials*, *178*(1–3), 10–28. https://doi.org/10.1016/j.jhazmat.2010.02.042

Benally, C., Messele, S. A., & Gamal El-Din, M. (2019). Adsorption of organic matter in oil sands process water (OSPW) by carbon xerogel. *Water Research*, *154*, 402–411. https://doi.org/10.1016/j.watres.2019.01.053

Brown, L. D., & Ulrich, A. C. (2015). Oil sands naphthenic acids: A review of properties, measurement, and treatment. *Chemosphere*, *127*, 276–290. https://doi.org/10.1016/j.chemosphere.2015.02.003

Buxton, G. V., Greenstock, C. L., Helman, W. P., & Ross, A. B. (1988). Critical Review of rate constants for reactions of hydrated electrons, hydrogen atoms and hydroxyl radicals (·OH/·O− in Aqueous Solution. *Journal of Physical and Chemical Reference Data*, *17*(2), 513–886. https://doi.org/10.1063/1.555805

Canadian Association of Petroleum Producers. (2020). *Statistical Handbook for Canada's Upstream Petroleum Industry*. Https://Www.Capp.ca/Wp-Content/Uploads/2020/02/Statistical-Handbook-2019-Data_357106.Pdf.

Canadian Council of Ministers of the Environment. (1987). *Canadian Water Quality Guidelines (CCREM)*. Https://Ccme.ca/En/Summary-Table.

Cancelli, A. M., & Gobas, F. A. P. C. (2022). Treatment of naphthenic acids in oil sands process-affected waters with a surface flow treatment wetland: mass removal, half-life, and toxicity-reduction. *Environmental Research*, *213*, 113755. https://doi.org/10.1016/j.envres.2022.113755

Cao, J., Lai, L., Lai, B., Yao, G., Chen, X., & Song, L. (2019). Degradation of tetracycline by peroxymonosulfate activated with zero-valent iron: Performance, intermediates, toxicity and mechanism. *Chemical Engineering Journal*, *364*, 45–56. https://doi.org/10.1016/j.cej.2019.01.113

Chen, C., Kuang, Y., Zhu, S., Burgert, I., Keplinger, T., Gong, A., Li, T., Berglund, L., Eichhorn, S. J., & Hu, L. (2020). Structure–property–function relationships of natural and engineered wood. *Nature Reviews Materials*, *5*(9), 642–666. https://doi.org/10.1038/s41578-020-0195-z

Chen, L., Li, F., Wei, Y., Li, G., Shen, K., & He, H.-J. (2019). High cadmium adsorption on nanoscale zero-valent iron coated Eichhornia crassipes biochar. *Environmental Chemistry Letters*, *17*(1), 589–594. https://doi.org/10.1007/s10311-018-0811-y

Chen, W., Zhang, X., Mamadiev, M., & Wang, Z. (2017). Sorption of perfluorooctane sulfonate and perfluorooctanoate on polyacrylonitrile fiber-derived activated carbon fibers: in comparison with activated carbon. *RSC Advances*, *7*(2), 927–938. https://doi.org/10.1039/C6RA25230C

Chia, C. H., Gong, B., Joseph, S. D., Marjo, C. E., Munroe, P., & Rich, A. M. (2012). Imaging of mineral-enriched biochar by FTIR, Raman and SEM–EDX. *Vibrational Spectroscopy*, *62*, 248–257. https://doi.org/10.1016/j.vibspec.2012.06.006

Cho, E.-J., Kang, J.-K., Moon, J.-K., Um, B.-H., Lee, C.-G., Jeong, S., & Park, S.-J. (2021). Removal of triclosan from aqueous solution via adsorption by kenaf-derived biochar: Its adsorption mechanism study via spectroscopic and experimental approaches. *Journal of Environmental Chemical Engineering*, *9*(6), 106343. https://doi.org/10.1016/j.jece.2021.106343

Clinical and Laboratory Standards Institute. (2018). *Methods for Dilution Antimicrobial Susceptibility Tests for Bacteria That Grow Aerobically* (11th ed.).

Crombie, K., Mašek, O., Sohi, S. P., Brownsort, P., & Cross, A. (2013). The effect of pyrolysis conditions on biochar stability as determined by three methods. *GCB Bioenergy*, *5*(2), 122–131. https://doi.org/10.1111/gcbb.12030

Cuervo Lumbaque, E., Lopes Tiburtius, E. R., Barreto-Rodrigues, M., & Sirtori, C. (2019). Current trends in the use of zero-valent iron (Fe0) for degradation of pharmaceuticals present in different water matrices. *Trends in Environmental Analytical Chemistry*, *24*, e00069. https://doi.org/10.1016/j.teac.2019.e00069

Cui, H.-J., Cai, J.-K., Zhao, H., Yuan, B., Ai, C., & Fu, M.-L. (2014). One step solvothermal synthesis of functional hybrid γ-Fe2O3/carbon hollow spheres with superior capacities for heavy metal removal. *Journal of Colloid and Interface Science*, *425*, 131–135. https://doi.org/10.1016/j.jcis.2014.03.049

Demir-Duz, H., Perez-Estrada, L. A., Álvarez, M. G., Gamal El-Din, M., & Contreras, S. (2022). O3/H2O2 and UV-C light irradiation treatment of oil sands process water.

Science of The Total Environment, *832*, 154804. https://doi.org/10.1016/j.scitotenv.2022.154804

Deng, J., Ya, C., Ge, Y., Cheng, Y., Chen, Y., Xu, M., & Wang, H. (2018). Activation of peroxymonosulfate by metal (Fe, Mn, Cu and Ni) doping ordered mesoporous Co_3O_4 for the degradation of enrofloxacin. *RSC Advances*, *8*(5), 2338–2349. https://doi.org/10.1039/C7RA07841B

Devi, P., & Saroha, A. K. (2015). Simultaneous adsorption and dechlorination of pentachlorophenol from effluent by Ni–ZVI magnetic biochar composites synthesized from paper mill sludge. *Chemical Engineering Journal*, *271*, 195–203. https://doi.org/10.1016/j.cej.2015.02.087

Doluweera, G., Kralovic, P., & Millington, D. (2017). *Economic Impacts of Canadian Oil and Gas Supply in Canada and the US*.

Dong, X., Ren, B., Sun, Z., Li, C., Zhang, X., Kong, M., Zheng, S., & Dionysiou, D. D. (2019). Monodispersed CuFe2O4 nanoparticles anchored on natural kaolinite as highly efficient peroxymonosulfate catalyst for bisphenol A degradation. *Applied Catalysis B: Environmental*, *253*, 206–217. https://doi.org/10.1016/j.apcatb.2019.04.052

dos Reis, G. S., Guy, M., Mathieu, M., Jebrane, M., Lima, E. C., Thyrel, M., Dotto, G. L., & Larsson, S. H. (2022). A comparative study of chemical treatment by MgCl2, ZnSO4, ZnCl2, and KOH on physicochemical properties and acetaminophen adsorption performance of biobased porous materials from tree bark residues. *Colloids and Surfaces A: Physicochemical and Engineering Aspects*, *642*, 128626. https://doi.org/10.1016/j.colsurfa.2022.128626

Egorova, K. S., & Ananikov, V. P. (2017). Toxicity of Metal Compounds: Knowledge and Myths. *Organometallics*, *36*(21), 4071–4090. https://doi.org/10.1021/acs.organomet.7b00605

Environment and Climate Change Canada. (2021). *National Inventory Report 1990 to 2021: Greenhouse Gas Sources and Sinks in Canada*. Publications.Gc.ca/Pub?Id=9.506002&sl=0.

Faheem, Du, J., Kim, S. H., Hassan, M. A., Irshad, S., & Bao, J. (2020). Application of biochar in advanced oxidation processes: supportive, adsorptive, and catalytic role. *Environmental Science and Pollution Research*, *27*(30), 37286–37312. https://doi.org/10.1007/s11356-020-07612-y

Fan, Q., Sun, J., Chu, L., Cui, L., Quan, G., Yan, J., Hussain, Q., & Iqbal, M. (2018). Effects of chemical oxidation on surface oxygen-containing functional groups and adsorption behavior of biochar. *Chemosphere*, *207*, 33–40. https://doi.org/10.1016/j.chemosphere.2018.05.044

Fang, Z., Chelme-Ayala, P., Shi, Q., Xu, C., & Gamal El-Din, M. (2018). Degradation of naphthenic acid model compounds in aqueous solution by UV activated persulfate: Influencing factors, kinetics and reaction mechanisms. *Chemosphere*, *211*, 271–277. https://doi.org/10.1016/j.chemosphere.2018.07.132

Fang, Z., Huang, R., Chelme-Ayala, P., Shi, Q., Xu, C., & Gamal El-Din, M. (2019). Comparison of UV/Persulfate and UV/H2O2 for the removal of naphthenic acids and acute toxicity towards Vibrio fischeri from petroleum production process water. *Science of The Total Environment*, *694*, 133686. https://doi.org/10.1016/j.scitotenv.2019.133686

Gamal El-Din, M., Fu, H., Wang, N., Chelme-Ayala, P., Pérez-Estrada, L., Drzewicz, P., Martin, J. W., Zubot, W., & Smith, D. W. (2011). Naphthenic acids speciation and removal during petroleum-coke adsorption and ozonation of oil sands process-affected water. *Science of The Total Environment*, *409*(23), 5119–5125. https://doi.org/10.1016/j.scitotenv.2011.08.033

Gao, A. L., & Wan, Y. (2023). Iron modified biochar enables recovery and recycling of phosphorus from wastewater through column filters and flow reactors. *Chemosphere*, *313*, 137434. https://doi.org/10.1016/j.chemosphere.2022.137434

Gao, L., Guo, Y., Zhan, J., Yu, G., & Wang, Y. (2022). Assessment of the validity of the quenching method for evaluating the role of reactive species in pollutant abatement during the persulfate-based process. *Water Research*, *221*, 118730. https://doi.org/10.1016/j.watres.2022.118730

Garcia-Garcia, E., Ge, J. Q., Oladiran, A., Montgomery, B., El-Din, M. G., Perez-Estrada, L. C., Stafford, J. L., Martin, J. W., & Belosevic, M. (2011). Ozone treatment ameliorates oil sands process water toxicity to the mammalian immune system. *Water Research*, *45*(18), 5849–5857. https://doi.org/10.1016/j.watres.2011.08.032

Gellert, G. (2000). Sensitivity and Significance of Luminescent Bacteria in Chronic Toxicity Testing Based on Growth and Bioluminescence. *Ecotoxicology and Environmental Safety*, *45*(1), 87–91. https://doi.org/10.1006/eesa.1999.1849

Ghanbari, F., & Moradi, M. (2017). Application of peroxymonosulfate and its activation methods for degradation of environmental organic pollutants: Review. *Chemical Engineering Journal*, *310*, 41–62. https://doi.org/10.1016/j.cej.2016.10.064

Ghodke, P. K., Sharma, A. K., Pandey, J. K., Chen, W.-H., Patel, A., & Ashokkumar, V. (2021). Pyrolysis of sewage sludge for sustainable biofuels and value-added biochar production. *Journal of Environmental Management*, *298*, 113450. https://doi.org/10.1016/j.jenvman.2021.113450

Government of Alberta. (2023, September 26). *Alberta crude oil reserves factsheet [2022 data]*. Https://Open.Alberta.ca/Publications/Alberta-Crude-Oil-Reserves-Factsheet.

Guo, Z., Chen, X., Hang, J., Li, Z., Zhong, C., Sun, A., Li, J., & Xu, S. (2023). Oxidative magnetization of biochar at relatively low pyrolysis temperature for efficient removal of different types of pollutants. *Bioresource Technology*, *387*, 129572. https://doi.org/10.1016/j.biortech.2023.129572

Hai, A., Bharath, G., Patah, M. F. A., Daud, W. M. A. W., K., R., Show, P., & Banat, F. (2023). Machine learning models for the prediction of total yield and specific surface area of biochar derived from agricultural biomass by pyrolysis. *Environmental Technology & Innovation*, *30*, 103071. https://doi.org/10.1016/j.eti.2023.103071

Hamid, Y., Liu, L., Usman, M., Naidu, R., Haris, M., Lin, Q., Ulhassan, Z., Hussain, M. I., & Yang, X. (2022). Functionalized biochars: Synthesis, characterization, and applications for removing trace elements from water. *Journal of Hazardous Materials*, *437*, 129337. https://doi.org/10.1016/j.jhazmat.2022.129337

Hasan, M. S., Vasquez, R., & Geza, M. (2021). Application of Biochar in Stormwater Treatment: Experimental and Modeling Investigation. *Processes*, *9*(5), 860. https://doi.org/10.3390/pr9050860

He, F., & Zhao, D. (2007). Manipulating the Size and Dispersibility of Zerovalent Iron Nanoparticles by Use of Carboxymethyl Cellulose Stabilizers. *Environmental Science & Technology*, *41*(17), 6216–6221. https://doi.org/10.1021/es0705543

He, Y., Patterson, S., Wang, N., Hecker, M., Martin, J. W., El-Din, M. G., Giesy, J. P., & Wiseman, S. B. (2012). Toxicity of untreated and ozone-treated oil sands process-affected water (OSPW) to early life stages of the fathead minnow (Pimephales promelas). *Water Research*, *46*(19), 6359–6368. https://doi.org/10.1016/j.watres.2012.09.004

Hernandez-Mena, L., Beraldo, A., & Pecora, A. (2014). Slow Pyrolysis of Bamboo Biomass: Analysis of Biochar Properties. *Chemical Engineering Transactions*, *37*, 115–120.

Heurtault, B. (2003). Physico-chemical stability of colloidal lipid particles. *Biomaterials*, *24*(23), 4283–4300. https://doi.org/10.1016/S0142-9612(03)00331-4

Honarmandrad, Z., Sun, X., Wang, Z., Naushad, M., & Boczkaj, G. (2023). Activated persulfate and peroxymonosulfate based advanced oxidation processes (AOPs) for antibiotics degradation – A review. *Water Resources and Industry*, *29*, 100194. https://doi.org/10.1016/j.wri.2022.100194

How, Z. T., Fang, Z., Chelme-Ayala, P., Ganiyu, S. O., Zhang, X., Xu, B., Chen, C., & Gamal El-Din, M. (2023). Ozone-activated peroxymonosulfate (O3/PMS) process for the removal of model naphthenic acids compounds: Kinetics, reactivity, and contribution of oxidative species. *Journal of Environmental Chemical Engineering*, *11*(3), 109935. https://doi.org/10.1016/j.jece.2023.109935

Hsu, C.-J., Cheng, Y.-H., Chung, A., Huang, Y.-P., Ting, Y., & Hsi, H.-C. (2023). Using recoverable sulfurized magnetic biochar for active capping to remediate multiple heavy

metal contaminated sediment. *Environmental Pollution*, *316*, 120555. https://doi.org/10.1016/j.envpol.2022.120555

Huang, R., McPhedran, K. N., & Gamal El-Din, M. (2015). Ultra Performance Liquid Chromatography Ion Mobility Time-of-Flight Mass Spectrometry Characterization of Naphthenic Acids Species from Oil Sands Process-Affected Water. *Environmental Science & Technology*, *49*(19), 11737–11745. https://doi.org/10.1021/acs.est.5b03178

Huang, R., Yang, L., How, Z. T., Fang, Z., Bekele, A., Letinski, D. J., Redman, A. D., & Gamal El-Din, M. (2021). Characterization of raw and ozonated oil sands process water utilizing atmospheric pressure gas chromatography time-of-flight mass spectrometry combined with solid phase microextractionun. *Chemosphere*, *266*, 129017. https://doi.org/10.1016/j.chemosphere.2020.129017

Huang, Z., Wang, T., Shen, M., Huang, Z., Chong, Y., & Cui, L. (2019). Coagulation treatment of swine wastewater by the method of in-situ forming layered double hydroxides and sludge recycling for preparation of biochar composite catalyst. *Chemical Engineering Journal*, *369*, 784–792. https://doi.org/10.1016/j.cej.2019.03.136

Hughes, S. A., Mahaffey, A., Shore, B., Baker, J., Kilgour, B., Brown, C., Peru, K. M., Headley, J. V., & Bailey, H. C. (2017). Using ultrahigh-resolution mass spectrometry and toxicity identification techniques to characterize the toxicity of oil sands process-affected water: The case for classical naphthenic acids. *Environmental Toxicology and Chemistry*, *36*(11), 3148–3157. https://doi.org/10.1002/etc.3892

Huong, P. T., Jitae, K., Al Tahtamouni, T. M., Le Minh Tri, N., Kim, H.-H., Cho, K. H., & Lee, C. (2020). Novel activation of peroxymonosulfate by biochar derived from rice

husk toward oxidation of organic contaminants in wastewater. *Journal of Water Process Engineering*, *33*, 101037. https://doi.org/10.1016/j.jwpe.2019.101037

Hussain, H., Green, I. R., & Ahmed, I. (2013). Journey Describing Applications of Oxone in Synthetic Chemistry. *Chemical Reviews*, *113*(5), 3329–3371. https://doi.org/10.1021/cr3004373

Inyang, M., & Dickenson, E. R. V. (2017). The use of carbon adsorbents for the removal of perfluoroalkyl acids from potable reuse systems. *Chemosphere*, *184*, 168–175. https://doi.org/10.1016/j.chemosphere.2017.05.161

Islam, M. S., McPhedran, K. N., Messele, S. A., Liu, Y., & Gamal El-Din, M. (2018). Isotherm and kinetic studies on adsorption of oil sands process-affected water organic compounds using granular activated carbon. *Chemosphere*, *202*, 716–725. https://doi.org/10.1016/j.chemosphere.2018.03.149

Islam, Md. S., Moreira, J., Chelme-Ayala, P., & Gamal El-Din, M. (2014). Prediction of naphthenic acid species degradation by kinetic and surrogate models during the ozonation of oil sands process-affected water. *Science of The Total Environment*, *493*, 282–290. https://doi.org/10.1016/j.scitotenv.2014.05.138

Jain, S., & Khare, P. (2017). Biochar: An Emerging Panacea for Contaminated and Degraded Soils. In *Green Technologies and Environmental Sustainability* (pp. 455–476). Springer International Publishing. https://doi.org/10.1007/978-3-319-50654-8_20

Jang, H. M., Yoo, S., Choi, Y.-K., Park, S., & Kan, E. (2018). Adsorption isotherm, kinetic modeling and mechanism of tetracycline on Pinus taeda-derived activated biochar. *Bioresource Technology*, *259*, 24–31. https://doi.org/10.1016/j.biortech.2018.03.013

Jerez, S., Ventura, M., Molina, R., Pariente, M. I., Martínez, F., & Melero, J. A. (2021). Comprehensive characterization of an oily sludge from a petrol refinery: A step forward for its valorization within the circular economy strategy. *Journal of Environmental Management*, *285*, 112124. https://doi.org/10.1016/j.jenvman.2021.112124

Ji, Z., Zhang, N., Huang, C., Duan, X., Ren, D., & Huo, Z. (2023). The Degradation of Polycyclic Aromatic Hydrocarbons (PAHs) by Ozone-Based Advanced Oxidation Processes: A Review. *Ozone: Science & Engineering*, 1–17. https://doi.org/10.1080/01919512.2023.2192751

Jieying Zheng, Zhao, Q., & Ye, Z. (2014). Preparation and characterization of activated carbon fiber (ACF) from cotton woven waste. *Applied Surface Science*, *299*, 86–91. https://doi.org/10.1016/j.apsusc.2014.01.190

Khuntia, B. K., Anwar, M. F., Alam, T., Samim, M., Kumari, M., & Arora, I. (2019). Synthesis and Characterization of Zero-Valent Iron Nanoparticles, and the Study of Their Effect against the Degradation of DDT in Soil and Assessment of Their Toxicity against Collembola and Ostracods. *ACS Omega*, *4*(20), 18502–18509. https://doi.org/10.1021/acsomega.9b01898

Kohantorabi, M., Moussavi, G., & Giannakis, S. (2021). A review of the innovations in metal- and carbon-based catalysts explored for heterogeneous peroxymonosulfate (PMS) activation, with focus on radical vs. non-radical degradation pathways of organic contaminants. *Chemical Engineering Journal*, *411*, 127957. https://doi.org/10.1016/j.cej.2020.127957

Kusic, H., Peternel, I., Ukic, S., Koprivanac, N., Bolanca, T., Papic, S., & Bozic, A. L. (2011). Modeling of iron activated persulfate oxidation treating reactive azo dye in water matrix.

Chemical Engineering Journal, *172*(1), 109–121. https://doi.org/10.1016/j.cej.2011.05.076

Lee, J. E., & Park, Y.-K. (2020). Applications of Modified Biochar-Based Materials for the Removal of Environment Pollutants: A Mini Review. *Sustainability*, *12*(15), 6112. https://doi.org/10.3390/su12156112

Lehmann, J., & Joseph, S. (2015). *Biochar for Environmental Management* (J. Lehmann & S. Joseph, Eds.). Routledge. https://doi.org/10.4324/9780203762264

Lévesque, C. M. (2014). *Oil sands process water and tailings pond contaminant transport and fate : physical, chemical and biological processes*. https://doi.org/10.14288/1.0165952

Li, C., Fu, L., Stafford, J., Belosevic, M., & Gamal El-Din, M. (2017). The toxicity of oil sands process-affected water (OSPW): A critical review. *Science of The Total Environment*, *601–602*, 1785–1802. https://doi.org/10.1016/j.scitotenv.2017.06.024

Li, H., Dong, X., da Silva, E. B., de Oliveira, L. M., Chen, Y., & Ma, L. Q. (2017). Mechanisms of metal sorption by biochars: Biochar characteristics and modifications. *Chemosphere*, *178*, 466–478. https://doi.org/10.1016/j.chemosphere.2017.03.072

Li, J., Zhang, Z., Xiang, Y., Jiang, J., & Yin, R. (2023). Role of UV-based advanced oxidation processes on NOM alteration and DBP formation in drinking water treatment: A state-of-the-art review. *Chemosphere*, *311*, 136870. https://doi.org/10.1016/j.chemosphere.2022.136870

Li, S., Yang, Y., Zheng, H., Zheng, Y., Jing, T., Ma, J., Nan, J., Leong, Y. K., & Chang, J.-S. (2022). Advanced oxidation process based on hydroxyl and sulfate radicals to degrade

refractory organic pollutants in landfill leachate. *Chemosphere*, *297*, 134214. https://doi.org/10.1016/j.chemosphere.2022.134214

Li, X., Wang, C., Zhang, J., Liu, J., Liu, B., & Chen, G. (2020). Preparation and application of magnetic biochar in water treatment: A critical review. *Science of The Total Environment*, *711*, 134847. https://doi.org/10.1016/j.scitotenv.2019.134847

Li, Y., Wu, Z., Zhao, C., Zhang, Y., Peng, D., & Gong, Z. (2023). Facile fabrication of Zero-valent-iron biochar from red mud for bisulfite activation in wastewater treatment: Performance and mechanism. *Environmental Technology & Innovation*, *30*, 103110. https://doi.org/10.1016/j.eti.2023.103110

Liang, C., & Su, H.-W. (2009). Identification of Sulfate and Hydroxyl Radicals in Thermally Activated Persulfate. *Industrial & Engineering Chemistry Research*, *48*(11), 5558–5562. https://doi.org/10.1021/ie9002848

Liu, J., Wang, L., Tang, J., & Ma, J. (2016). Photocatalytic degradation of commercially sourced naphthenic acids by TiO2-graphene composite nanomaterial. *Chemosphere*, *149*, 328–335. https://doi.org/10.1016/j.chemosphere.2016.01.074

Liu, Y., He, Z., & Uchimiya, M. (2015). Comparison of Biochar Formation from Various Agricultural By-Products Using FTIR Spectroscopy. *Modern Applied Science*, *9*(4). https://doi.org/10.5539/mas.v9n4p246

Ma, W., Xu, Y., Zhou, D., Wang, L., Liang, X., & Sun, Y. (2023). Development and optimization of high–performance nano–biochar for efficient removal Cd in aqueous: Absorption performance and interaction mechanisms. *Chemical Engineering Research and Design*, *189*, 516–529. https://doi.org/10.1016/j.cherd.2022.11.051

Mallah, M. A., Changxing, L., Mallah, M. A., Noreen, S., Liu, Y., Saeed, M., Xi, H., Ahmed, B., Feng, F., Mirjat, A. A., Wang, W., Jabar, A., Naveed, M., Li, J.-H., & Zhang, Q. (2022). Polycyclic aromatic hydrocarbon and its effects on human health: An overeview. *Chemosphere*, *296*, 133948. https://doi.org/10.1016/j.chemosphere.2022.133948

Manasfi, T. (2021). *Ozonation in drinking water treatment: an overview of general and practical aspects, mechanisms, kinetics, and byproduct formation* (pp. 85–116). https://doi.org/10.1016/bs.coac.2021.02.003

Martin, J. W., Han, X., Peru, K. M., & Headley, J. V. (2008). Comparison of high- and low-resolution electrospray ionization mass spectrometry for the analysis of naphthenic acid mixtures in oil sands process water. *Rapid Communications in Mass Spectrometry*, *22*(12), 1919–1924. https://doi.org/10.1002/rcm.3570

Medeiros, D. C. C. da S., Chelme-Ayala, P., & Gamal El-Din, M. (2023). Sludge-based activated biochar for adsorption treatment of real oil sands process water: Selectivity of naphthenic acids, reusability of spent biochar, leaching potential, and acute toxicity removal. *Chemical Engineering Journal*, *463*. https://doi.org/10.1016/j.cej.2023.142329

Medeiros, D. C. C. da S., Nzediegwu, C., Benally, C., Messele, S. A., Kwak, J. H., Naeth, M. A., Ok, Y. S., Chang, S. X., & Gamal El-Din, M. (2022). Pristine and engineered biochar for the removal of contaminants co-existing in several types of industrial wastewaters: A critical review. *Science of The Total Environment*, *809*, 151120. https://doi.org/10.1016/J.SCITOTENV.2021.151120

Meng, F., Wang, Y., & Cao, Q. (2023). Synergistic enhancement of redox pairs and functional groups for the removal of phenolic organic pollutants by activated PMS using silica-

composited biochar: Mechanism and environmental toxicity assessment. *Chemosphere*, *337*, 139441. https://doi.org/10.1016/j.chemosphere.2023.139441

Meng, L., How, Z. T., Chelme-Ayala, P., Benally, C., & Gamal El-Din, M. (2023). Z-scheme plasmonic Ag decorated Bi2WO6/NiO hybrids for enhanced photocatalytic treatment of naphthenic acids in real oil sands process water under simulated solar irradiation. *Journal of Hazardous Materials*, *454*, 131441. https://doi.org/10.1016/j.jhazmat.2023.131441

Meshref, M. N. A., Chelme-Ayala, P., & Gamal El-Din, M. (2017). Fate and abundance of classical and heteroatomic naphthenic acid species after advanced oxidation processes: Insights and indicators of transformation and degradation. *Water Research*, *125*, 62–71. https://doi.org/10.1016/j.watres.2017.08.007

Mohammed, N. A. S., Abu-Zurayk, R. A., Hamadneh, I., & Al-Dujaili, A. H. (2018). Phenol adsorption on biochar prepared from the pine fruit shells: Equilibrium, kinetic and thermodynamics studies. *Journal of Environmental Management*, *226*, 377–385. https://doi.org/10.1016/j.jenvman.2018.08.033

Morgan, D. J. (2021). Comments on the XPS Analysis of Carbon Materials. *C*, *7*(3), 51. https://doi.org/10.3390/c7030051

Natural Resources Canada. (2022). *What are the oil sands?* Https://Natural-Resources.Canada.ca/Our-Natural-Resources/Energy-Sources-Distribution/Fossil-Fuels/Crude-Oil/What-Are-Oil-Sands/18089.

Natural Resources Canada. (2023). *Energy Fact Book*. Https://Publications.Gc.ca/Collections/Collection_2022/Rncan-Nrcan/M136-1-2022-Eng.Pdf.

Nguyen, V.-T., Vo, T.-D.-H., Nguyen, T.-B., Dat, N. D., Huu, B. T., Nguyen, X.-C., Tran, T., Le, T.-N.-C., Duong, T.-G.-H., Bui, M.-H., Dong, C.-D., & Bui, X.-T. (2022). Adsorption of norfloxacin from aqueous solution on biochar derived from spent coffee ground: Master variables and response surface method optimized adsorption process. *Chemosphere*, *288*, 132577. https://doi.org/10.1016/j.chemosphere.2021.132577

Nzediegwu, C., Arshad, M., Ulah, A., Naeth, M. A., & Chang, S. X. (2021). Fuel, thermal and surface properties of microwave-pyrolyzed biochars depend on feedstock type and pyrolysis temperature. *Bioresource Technology*, *320*, 124282. https://doi.org/10.1016/j.biortech.2020.124282

Nzediegwu, C., Naeth, M. A., & Chang, S. X. (2021). Carbonization temperature and feedstock type interactively affect chemical, fuel, and surface properties of hydrochars. *Bioresource Technology*, *330*, 124976. https://doi.org/10.1016/j.biortech.2021.124976

Oh, W.-D., Dong, Z., & Lim, T.-T. (2016). Generation of sulfate radical through heterogeneous catalysis for organic contaminants removal: Current development, challenges and prospects. *Applied Catalysis B: Environmental*, *194*, 169–201. https://doi.org/10.1016/j.apcatb.2016.04.003

Oh, W.-D., & Lim, T.-T. (2019). Design and application of heterogeneous catalysts as peroxydisulfate activator for organics removal: An overview. *Chemical Engineering Journal*, *358*, 110–133. https://doi.org/10.1016/j.cej.2018.09.203

Oil and Gas Journal. (2022). Worldwide Look at Reserves and Production. *Oil and Gas Journal*.

Oliveira, F. R., Patel, A. K., Jaisi, D. P., Adhikari, S., Lu, H., & Khanal, S. K. (2017). Environmental application of biochar: Current status and perspectives. *Bioresource Technology*, *246*, 110–122. https://doi.org/10.1016/j.biortech.2017.08.122

Pap, S., Shearer, L., & Gibb, S. W. (2023). Effective removal of metformin from water using an iron-biochar composite: Mechanistic studies and performance optimisation. *Journal of Environmental Chemical Engineering*, *11*(5), 110360. https://doi.org/10.1016/j.jece.2023.110360

Pardoe, H., Chua-anusorn, W., St. Pierre, T. G., & Dobson, J. (2001). Structural and magnetic properties of nanoscale iron oxide particles synthesized in the presence of dextran or polyvinyl alcohol. *Journal of Magnetism and Magnetic Materials*, *225*(1–2), 41–46. https://doi.org/10.1016/S0304-8853(00)01226-9

Parsons, S. (2015). Advanced Oxidation Processes for Water and Wastewater Treatment. *Water Intelligence Online*, *4*(0), 9781780403076–9781780403076. https://doi.org/10.2166/9781780403076

Peng, X., Liu, X., Zhou, Y., Peng, B., Tang, L., Luo, L., Yao, B., Deng, Y., Tang, J., & Zeng, G. (2017). New insights into the activity of a biochar supported nanoscale zerovalent iron composite and nanoscale zero valent iron under anaerobic or aerobic conditions. *RSC Advances*, *7*(15), 8755–8761. https://doi.org/10.1039/C6RA27256H

Pereira, A. S., Islam, M. S., Gamal El-Din, M., & Martin, J. W. (2013). Ozonation degrades all detectable organic compound classes in oil sands process-affected water; an application of high-performance liquid chromatography/obitrap mass spectrometry. *Rapid Communications in Mass Spectrometry*, *27*(21), 2317–2326. https://doi.org/10.1002/rcm.6688

Phenrat, T., Saleh, N., Sirk, K., Tilton, R. D., & Lowry, G. V. (2007). Aggregation and Sedimentation of Aqueous Nanoscale Zerovalent Iron Dispersions. *Environmental Science & Technology*, *41*(1), 284–290. https://doi.org/10.1021/es061349a

Ponder, S. M., Darab, J. G., & Mallouk, T. E. (2000). Remediation of Cr(VI) and Pb(II) Aqueous Solutions Using Supported, Nanoscale Zero-valent Iron. *Environmental Science & Technology*, *34*(12), 2564–2569. https://doi.org/10.1021/es9911420

Pourrezaei, P., Alpatova, A., Chelme-Ayala, P., Perez-Estrada, L. A., Jensen-Fontaine, M., Le, X. C., & Gamal El-Din, M. (2014). Impact of petroleum coke characteristics on the adsorption of the organic fractions from oil sands process-affected water. *International Journal of Environmental Science and Technology*, *11*(7), 2037–2050. https://doi.org/10.1007/S13762-013-0406-X/METRICS

Premarathna, K. S. D., Rajapaksha, A. U., Sarkar, B., Kwon, E. E., Bhatnagar, A., Ok, Y. S., & Vithanage, M. (2019). Biochar-based engineered composites for sorptive decontamination of water: A review. *Chemical Engineering Journal*, *372*, 536–550. https://doi.org/10.1016/j.cej.2019.04.097

Quinlan, P. J., & Tam, K. C. (2015). Water treatment technologies for the remediation of naphthenic acids in oil sands process-affected water. *Chemical Engineering Journal*, *279*, 696–714. https://doi.org/10.1016/j.cej.2015.05.062

Rastogi, A., Al-Abed, S. R., & Dionysiou, D. D. (2009). Sulfate radical-based ferrous–peroxymonosulfate oxidative system for PCBs degradation in aqueous and sediment systems. *Applied Catalysis B: Environmental*, *85*(3–4), 171–179. https://doi.org/10.1016/j.apcatb.2008.07.010

Redman, A. D., Butler, J. D., Letinski, D. J., Di Toro, D. M., Leon Paumen, M., & Parkerton, T. F. (2018). Technical basis for using passive sampling as a biomimetic extraction procedure to assess bioavailability and predict toxicity of petroleum substances. *Chemosphere*, *199*, 585–594. https://doi.org/10.1016/j.chemosphere.2018.02.024

Richely, E., Nuez, L., Pérez, J., Rivard, C., Baley, C., Bourmaud, A., Guessasma, S., & Beaugrand, J. (2022). Influence of defects on the tensile behaviour of flax fibres: Cellulose microfibrils evolution by synchrotron X-ray diffraction and finite element modelling. *Composites Part C: Open Access*, *9*, 100300. https://doi.org/10.1016/j.jcomc.2022.100300

Saha, P., Zhou, C., Moradi, M., Rijnaarts, H. H. M., & Bruning, H. (2023). Heat-activated peroxydisulfate and peroxymonosulfate-mediated degradation of benzotriazole: Effects of chloride on kinetics, pathways and transformation product toxicity. *Chemical Engineering Journal Advances*, *14*, 100472. https://doi.org/10.1016/j.ceja.2023.100472

Sánchez-Montes, I., Mokarizadeh, H., Paul, S., Moghrabi, K., Hussain, N., Chelme-Ayala, P., Stafford, J. L., Lanza, M. R. V., & Gamal El-Din, M. (2024). UVA LED-assisted breakdown of persulfate oxidants for the treatment of real oil sands process water: Removal of naphthenic acids and evaluation of residual toxicity. *Chemical Engineering Journal*, *481*, 148631. https://doi.org/10.1016/j.cej.2024.148631

Sánchez-Montes, I., O. S. Santos, G., O. Silva, T., Colombo, R., & R. V. Lanza, M. (2023). An innovative approach to the application of electrochemical processes based on the in-situ generation of H2O2 for water treatment. *Journal of Cleaner Production*, *392*, 136242. https://doi.org/10.1016/j.jclepro.2023.136242

Sánchez-Montes, I., Santos, G. O. S., dos Santos, A. J., Fernandes, C. H. M., Souto, R. S., Chelme-Ayala, P., El-Din, M. G., & Lanza, M. R. V. (2023). Toxicological aspect of water treated by chlorine-based advanced oxidation processes: A review. *Science of The Total Environment*, *878*, 163047. https://doi.org/10.1016/j.scitotenv.2023.163047

Schramm, L. L., Stasiuk, E. N., & MacKinnon, M. (2000). Surfactants in Athabasca Oil Sands Slurry Conditioning, Flotation Recovery, and Tailings Processes. In *Surfactants* (pp. 365–430). Cambridge University Press. https://doi.org/10.1017/CBO9780511524844.011

Shen, L., Wang, J., Li, Z., Fan, L., Chen, R., Wu, X., Li, J., & Zeng, W. (2020). A high-efficiency Fe2O3@Microalgae composite for heavy metal removal from aqueous solution. *Journal of Water Process Engineering*, *33*, 101026. https://doi.org/10.1016/j.jwpe.2019.101026

Shi, J., Dai, B., Shen, X., Xu, L., Zhang, Y., & Gan, L. (2023). Wood induced preparation of Fe3C decorated biochar for peroxymonosulfate activation towards bisphenol a degradation with low ion leaching. *Journal of Environmental Management*, *340*, 117978. https://doi.org/10.1016/j.jenvman.2023.117978

Shu, Z., Li, C., Belosevic, M., Bolton, J. R., & El-Din, M. G. (2014). Application of a Solar UV/Chlorine Advanced Oxidation Process to Oil Sands Process-Affected Water Remediation. *Environmental Science & Technology*, *48*(16), 9692–9701. https://doi.org/10.1021/es5017558

Silvestri, D., Wacławek, S., Venkateshaiah, A., Krawczyk, K., Sobel, B., Padil, V. V. T., Černík, M., & Varma, R. S. (2020). Synthesis of Ag nanoparticles by a chitosan-poly(3-

hydroxybutyrate) polymer conjugate and their superb catalytic activity. *Carbohydrate Polymers*, *232*, 115806. https://doi.org/10.1016/j.carbpol.2019.115806

Song, J., How, Z. T., Huang, Z., & Gamal El-Din, M. (2022). Biochar/iron oxide composite as an efficient peroxymonosulfate catalyst for the degradation of model naphthenic acids compounds. *Chemical Engineering Journal*, *429*, 132220. https://doi.org/10.1016/j.cej.2021.132220

Statistics Canada. (2023). *Table 25-10-0063-01 Supply and disposition of crude oil and equivalent*. Https://Doi.Org/10.25318/2510006301-Eng.

Suara, M. A., Ganiyu, S. O., Paul, S., Stafford, J. L., & Gamal El-Din, M. (2022). Solar-activated zinc oxide photocatalytic treatment of real oil sands process water: Effect of treatment parameters on naphthenic acids, polyaromatic hydrocarbons and acute toxicity removal. *Science of The Total Environment*, *819*, 153029. https://doi.org/10.1016/j.scitotenv.2022.153029

Sun, H., & Wang, S. (2015). *Chapter 6. Catalytic oxidation of organic pollutants in aqueous solution using sulfate radicals* (pp. 209–247). https://doi.org/10.1039/9781782622697-00209

Sun, H., Zhang, B., Wang, N., Zhang, N., Ma, Y., Zang, L., Li, Z., & Xue, R. (2023). Refractory organics removal in PMS and H2O2/PMS oxidation system activated by biochar/nZVI/MoS2 composite: Synthesis, performance, mechanism and dosing methods. *Journal of Environmental Chemical Engineering*, *11*(1), 109134. https://doi.org/10.1016/j.jece.2022.109134

Sun, M., Wang, C., Luo, Z., & Zhu, X. (2023). Synthesis of magnetic biochar with high iron content and large specific surface area: Synergistic effect of Fe doping and KOH

activation. *Journal of Analytical and Applied Pyrolysis*, *173*, 106096. https://doi.org/10.1016/j.jaap.2023.106096

Sun, N., Chelme-Ayala, P., Klamerth, N., McPhedran, K. N., Islam, Md. S., Perez-Estrada, L., Drzewicz, P., Blunt, B. J., Reichert, M., Hagen, M., Tierney, K. B., Belosevic, M., & Gamal El-Din, M. (2014). Advanced Analytical Mass Spectrometric Techniques and Bioassays to Characterize Untreated and Ozonated Oil Sands Process-Affected Water. *Environmental Science & Technology*, *48*(19), 11090–11099. https://doi.org/10.1021/es503082j

Sun, Y., Yu, I. K. M., Tsang, D. C. W., Cao, X., Lin, D., Wang, L., Graham, N. J. D., Alessi, D. S., Komárek, M., Ok, Y. S., Feng, Y., & Li, X.-D. (2019). Multifunctional iron-biochar composites for the removal of potentially toxic elements, inherent cations, and hetero-chloride from hydraulic fracturing wastewater. *Environment International*, *124*, 521–532. https://doi.org/10.1016/j.envint.2019.01.047

Tan, C., Dong, Y., Fu, D., Gao, N., Ma, J., & Liu, X. (2018). Chloramphenicol removal by zero valent iron activated peroxymonosulfate system: Kinetics and mechanism of radical generation. *Chemical Engineering Journal*, *334*, 1006–1015. https://doi.org/10.1016/j.cej.2017.10.020

Tang, W. Z. (2003). *Physicochemical Treatment of Hazardous Wastes*. CRC Press. https://doi.org/10.1201/9780203506219

Teixeira, L. A. C., Andia, J. P. M., Yokoyama, L., da Fonseca Araújo, F. V., & Sarmiento, C. M. (2013). Oxidation of cyanide in effluents by Caro's Acid. *Minerals Engineering*, *45*, 81–87. https://doi.org/10.1016/j.mineng.2013.01.008

Tufail, A., Price, W. E., & Hai, F. I. (2020). A critical review on advanced oxidation processes for the removal of trace organic contaminants: A voyage from individual to integrated processes. *Chemosphere*, *260*, 127460. https://doi.org/10.1016/j.chemosphere.2020.127460

Uttran, A. (2018). Adsorption of NPK fertilizer and humic acid on palm kernel shell biochar. *Journal of Oil Palm Research*. https://doi.org/10.21894/jopr.2018.0029

Vincent Crist. (2018). *The international XPS database*. Https://Xpsdatabase.Com/.

Wan, J., Chakraborty, T., Xu, C. (Charles), & Ray, M. B. (2019). Treatment train for tailings pond water using Opuntia ficus-indica as coagulant. *Separation and Purification Technology*, *211*, 448–455. https://doi.org/10.1016/j.seppur.2018.09.083

Wang, C., Klamerth, N., Messele, S. A., Singh, A., Belosevic, M., & Gamal El-Din, M. (2016). Comparison of UV/hydrogen peroxide, potassium ferrate(VI), and ozone in oxidizing the organic fraction of oil sands process-affected water (OSPW). *Water Research*, *100*, 476–485. https://doi.org/10.1016/j.watres.2016.05.037

Wang, J., Shen, M., Gong, Q., Wang, X., Cai, J., Wang, S., & Chen, Z. (2020). One-step preparation of ZVI-sludge derived biochar without external source of iron and its application on persulfate activation. *Science of The Total Environment*, *714*, 136728. https://doi.org/10.1016/j.scitotenv.2020.136728

Wang, J., & Wang, S. (2018). Activation of persulfate (PS) and peroxymonosulfate (PMS) and application for the degradation of emerging contaminants. *Chemical Engineering Journal*, *334*, 1502–1517. https://doi.org/10.1016/j.cej.2017.11.059

Wang, K.-S., Lin, C.-L., Wei, M.-C., Liang, H.-H., Li, H.-C., Chang, C.-H., Fang, Y.-T., & Chang, S.-H. (2010). Effects of dissolved oxygen on dye removal by zero-valent iron.

Journal of Hazardous Materials, *182*(1–3), 886–895. https://doi.org/10.1016/j.jhazmat.2010.07.002

Wang, N., Chelme-Ayala, P., Perez-Estrada, L., Garcia-Garcia, E., Pun, J., Martin, J. W., Belosevic, M., & Gamal El-Din, M. (2013). Impact of Ozonation on Naphthenic Acids Speciation and Toxicity of Oil Sands Process-Affected Water to *Vibrio fischeri* and Mammalian Immune System. *Environmental Science & Technology*, *47*(12), 6518–6526. https://doi.org/10.1021/es4008195

Wang, S., Zhao, M., Zhou, M., Li, Y. C., Wang, J., Gao, B., Sato, S., Feng, K., Yin, W., Igalavithana, A. D., Oleszczuk, P., Wang, X., & Ok, Y. S. (2019). Biochar-supported nZVI (nZVI/BC) for contaminant removal from soil and water: A critical review. *Journal of Hazardous Materials*, *373*, 820–834. https://doi.org/10.1016/j.jhazmat.2019.03.080

Wang, Y. R., & Chu, W. (2011). Degradation of a xanthene dye by Fe(II)-mediated activation of Oxone process. *Journal of Hazardous Materials*, *186*(2–3), 1455–1461. https://doi.org/10.1016/j.jhazmat.2010.12.033

Whale, G. F., Hjort, M., Di Paolo, C., Redman, A. D., Postma, J. F., Legradi, J., & Leonards, P. E. G. (2022). Assessment of oil refinery wastewater and effluent integrating bioassays, mechanistic modelling and bioavailability evaluation. *Chemosphere*, *287*, 132146. https://doi.org/10.1016/j.chemosphere.2021.132146

Williams, A. T. R., Winfield, S. A., & Miller, J. N. (1983). Relative fluorescence quantum yields using a computer-controlled luminescence spectrometer. *The Analyst*, *108*(1290), 1067. https://doi.org/10.1039/an9830801067

Wiseman, S. B., Anderson, J. C., Liber, K., & Giesy, J. P. (2013). Endocrine disruption and oxidative stress in larvae of Chironomus dilutus following short-term exposure to fresh or aged oil sands process-affected water. *Aquatic Toxicology*, *142–143*, 414–421. https://doi.org/10.1016/j.aquatox.2013.09.003

Wiseman, S. B., He, Y., Gamal-El Din, M., Martin, J. W., Jones, P. D., Hecker, M., & Giesy, J. P. (2013). Transcriptional responses of male fathead minnows exposed to oil sands process-affected water. *Comparative Biochemistry and Physiology Part C: Toxicology & Pharmacology*, *157*(2), 227–235. https://doi.org/10.1016/j.cbpc.2012.12.002

Xia, D., Tan, F., Zhang, C., Jiang, X., Chen, Z., Li, H., Zheng, Y., Li, Q., & Wang, Y. (2016). ZnCl 2 -activated biochar from biogas residue facilitates aqueous As(III) removal. *Applied Surface Science*, *377*, 361–369. https://doi.org/10.1016/j.apsusc.2016.03.109

Xiao, R., Luo, Z., Wei, Z., Luo, S., Spinney, R., Yang, W., & Dionysiou, D. D. (2018). Activation of peroxymonosulfate/persulfate by nanomaterials for sulfate radical-based advanced oxidation technologies. *Current Opinion in Chemical Engineering*, *19*, 51–58. https://doi.org/10.1016/j.coche.2017.12.005

Xiao, S., Cheng, M., Zhong, H., Liu, Z., Liu, Y., Yang, X., & Liang, Q. (2020). Iron-mediated activation of persulfate and peroxymonosulfate in both homogeneous and heterogeneous ways: A review. *Chemical Engineering Journal*, *384*, 123265. https://doi.org/10.1016/j.cej.2019.123265

Xu, W., Liang, J., Li, J., Pillai, S. C., Liang, F., Li, M., Xiao, K., Li, J., Wang, Y., Jiang, X., Liu, Z., Beiyuan, J., & Wang, H. (2024). Biochar encapsulated metal nanoflowers for high efficient degradation of metronidazole via peroxymonosulfate activation.

Separation and Purification Technology, *328*, 125081. https://doi.org/10.1016/j.seppur.2023.125081

Xue, J., Huang, C., Zhang, Y., Liu, Y., & Gamal El-Din, M. (2018). Bioreactors for oil sands process-affected water (OSPW) treatment: A critical review. *Science of The Total Environment*, *627*, 916–933. https://doi.org/10.1016/j.scitotenv.2018.01.292

Yan, J., Han, L., Gao, W., Xue, S., & Chen, M. (2015). Biochar supported nanoscale zerovalent iron composite used as persulfate activator for removing trichloroethylene. *Bioresource Technology*, *175*, 269–274. https://doi.org/10.1016/j.biortech.2014.10.103

Yan, Q., Wan, C., Liu, J., Gao, J., Yu, F., Zhang, J., & Cai, Z. (2013). Iron nanoparticles in situ encapsulated in biochar-based carbon as an effective catalyst for the conversion of biomass-derived syngas to liquid hydrocarbons. *Green Chemistry*, *15*(6), 1631. https://doi.org/10.1039/c3gc37107g

Zani, C., Feretti, D., Buschini, A., Poli, P., Rossi, C., Guzzella, L., Caterino, F. Di, & Monarca, S. (2005). Toxicity and genotoxicity of surface water before and after various potabilization steps. *Mutation Research/Genetic Toxicology and Environmental Mutagenesis*, *587*(1–2), 26–37. https://doi.org/10.1016/j.mrgentox.2005.07.006

Zhang, G., Huang, D., Cheng, M., Lei, L., Chen, S., Wang, R., Xue, W., Liu, Y., Chen, Y., & Li, Z. (2020). Megamerger of MOFs and g-C_3N_4 for energy and environment applications: upgrading the framework stability and performance. *Journal of Materials Chemistry A*, *8*(35), 17883–17906. https://doi.org/10.1039/D0TA05662F

Zhang, T., Yang, Y., Gao, J., Li, X., Yu, H., Wang, N., Du, P., Yu, R., Li, H., Fan, X., & Zhou, Z. (2020). Synergistic degradation of chloramphenicol by ultrasound-enhanced

nanoscale zero-valent iron/persulfate treatment. *Separation and Purification Technology*, *240*, 116575. https://doi.org/10.1016/j.seppur.2020.116575

Zhang, Y., Klamerth, N., Messele, S. A., Chelme-Ayala, P., & Gamal El-Din, M. (2016). Kinetics study on the degradation of a model naphthenic acid by ethylenediamine-N,N'-disuccinic acid-modified Fenton process. *Journal of Hazardous Materials*, *318*, 371–378. https://doi.org/10.1016/j.jhazmat.2016.06.063

Zhang, Y., Xiangshi, P., Tian, J., Li, F., Fan, X., Ma, L., & Zhang, R. (2021). Synthesis of peroxymonosulfate composite catalyst (Fe0/Fe3O4/biochar) using waterworks sludge and walnut shell for degrading methylene blue. *Journal of Environmental Chemical Engineering*, *9*(6), 106856. https://doi.org/10.1016/j.jece.2021.106856

Zhao, C., Shao, B., Yan, M., Liu, Z., Liang, Q., He, Q., Wu, T., Liu, Y., Pan, Y., Huang, J., Wang, J., Liang, J., & Tang, L. (2021). Activation of peroxymonosulfate by biochar-based catalysts and applications in the degradation of organic contaminants: A review. *Chemical Engineering Journal*, *416*, 128829. https://doi.org/10.1016/j.cej.2021.128829

Zhao, L., Cao, X., Mašek, O., & Zimmerman, A. (2013). Heterogeneity of biochar properties as a function of feedstock sources and production temperatures. *Journal of Hazardous Materials*, *256–257*, 1–9. https://doi.org/10.1016/j.jhazmat.2013.04.015

Zhao, Q., Mao, Q., Zhou, Y., Wei, J., Liu, X., Yang, J., Luo, L., Zhang, J., Chen, H., Chen, H., & Tang, L. (2017). Metal-free carbon materials-catalyzed sulfate radical-based advanced oxidation processes: A review on heterogeneous catalysts and applications. *Chemosphere*, *189*, 224–238. https://doi.org/10.1016/j.chemosphere.2017.09.042

Zheng, X., Niu, X., Zhang, D., Lv, M., Ye, X., Ma, J., Lin, Z., & Fu, M. (2022). Metal-based catalysts for persulfate and peroxymonosulfate activation in heterogeneous ways: A

review. *Chemical Engineering Journal*, *429*, 132323. https://doi.org/10.1016/J.CEJ.2021.132323

Zhou, Q., Song, C., Wang, P., Zhao, Z., Li, Y., & Zhan, S. (2023). Generating dual-active species by triple-atom sites through peroxymonosulfate activation for treating micropollutants in complex water. *Proceedings of the National Academy of Sciences*, *120*(13). https://doi.org/10.1073/pnas.2300085120

Zubot, W., MacKinnon, M. D., Chelme-Ayala, P., Smith, D. W., & Gamal El-Din, M. (2012). Petroleum coke adsorption as a water management option for oil sands process-affected water. *Science of The Total Environment*, *427–428*, 364–372. https://doi.org/10.1016/j.scitotenv.2012.04.024